
Diffusion-EDFs: Bi-equivariant Denoising Generative Modeling on SE(3) for Visual Robotic Manipulation

Hyunwoo Ryu¹, Jiwoo Kim¹, Junwoo Chang¹, Hyun Seok Ahn¹
 Joohwan Seo², Taehan Kim³, Yubin Kim⁴, Jongeun Choi^{1,2,*}, Roberto Horowitz²,
¹Yonsei University, ²University of California, Berkeley,
³Samsung Research, ⁴Massachusetts Institute of Technology
 {tomato1mule, nfsshift9801, junwoochang, hs991210, jongeunchoi}@yonsei.ac.kr
 {joohwan_seo, horowitz}@berkeley.edu
 taehan11.kim@samsung.com, ybkim95@media.mit.edu,

Abstract

Recent studies have verified that equivariant methods can significantly improve the data efficiency, generalizability, and robustness in robot learning. Meanwhile, denoising diffusion-based generative modeling has recently gained significant attention as a promising approach for robotic manipulation learning from demonstrations with stochastic behaviors. In this paper, we present *Diffusion-EDFs*, a novel approach that incorporates spatial roto-translation equivariance, i.e., $SE(3)$ -equivariance to diffusion generative modeling. By integrating $SE(3)$ -equivariance into our model architectures, we demonstrate that our proposed method exhibits remarkable data efficiency, requiring only 5 to 10 task demonstrations for effective end-to-end training. Furthermore, our approach showcases superior generalizability compared to previous diffusion-based manipulation methods. Codes are available at: https://github.com/tomato1mule/diffusion_edf

1 Introduction

Denoising diffusion-based generative models are increasingly being recognized as superior methods for modeling stochastic and multimodal policies [1–11]. In particular, *SE(3)-Diffusion Fields* [7] apply diffusion-based learning on the $SE(3)$ manifold to generate grasp poses of the end-effector. However, while being proficient at learning highly stochastic behaviors, current diffusion-based approaches require significant amount of demonstration data for training.

On the other hand, extensive work has shown that incorporating equivariance can significantly enhance the data efficiency, generalizability, and robustness in robot learning [12–21, 9, 10]. In particular, several recent works explore the use of $SE(3)$ -equivariant models for learning 6-DoF manipulation tasks from point cloud observations [15, 13, 14, 19, 17]. *Equivariant Descriptor Fields* (EDFs) [19] achieve few-shot level data efficiency and generalizability in 6-DoF manipulation learning by employing an $SE(3)$ *bi-equivariant* [19, 20] energy-based model (EBM). EDFs are distinguished from other $SE(3)$ -equivariant methods in that they can be trained and deployed in a fully end-to-end manner without requiring any pre-training or object segmentation. However, training energy-based models is typically slow and unstable due to the Markov Chain Monte Carlo sampling. For instance, more than 10 hours are generally required for EDFs to stably learn only a few task demonstrations. On the other hand, training is significantly faster and more stable for diffusion models. Consequently, $SE(3)$ -equivariant diffusion-based generative modeling is highly desirable.

*Corresponding author: Jongeun Choi (jungeunchoi@yonsei.ac.kr)

In this paper, we present *Diffusion-EDFs* for bi-equivariant diffusion generative modeling on the $SE(3)$ -manifold. Bi-equivariance [19, 20] requires the model to be equivariant to both the objects in the scene and grasp (see Appendix A), enabling previously learned policies to be generalized to novel object configurations. We first begin by formally discussing the required conditions for achieving bi-equivariance in diffusion models. Next, we provide novel practical methods to address the challenges that are posed to meet these conditions. Finally, we validate the data efficiency, robustness, and generalizability of Diffusion-EDFs by comparing them to other state-of-the-art methods.

2 Preliminaries

2.1 SO(3) Group Representation Theory

A *representation* $\mathbf{D}(g)$ is a map from a group \mathcal{G} to a linear map on a vector space \mathcal{W} that is homomorphic to the group action such that

$$\mathbf{D}(g)\mathbf{D}(h) = \mathbf{D}(gh) \quad \forall g, h \in \mathcal{G} \quad (1)$$

The vector space \mathcal{W} where $\mathbf{D}(g)$ acts on is called the *representation space* of $\mathbf{D}(g)$. Two representations $\mathbf{D}(g)$ and $\mathbf{D}'(g)$ are said to be *equivalent* (not to be confused with *equivariant*) if there exists a change of basis W such that $\mathbf{D}(g) = W\mathbf{D}'(g)W^{-1}$. A representation is said to be *reducible* if it is equivalent to a block-diagonal of smaller representations. *Irreducible representations*, or *irreps* are representations that cannot be reduced anymore. Hence, irreps are the building blocks of any larger representation of \mathcal{G} . We follow the E3NN [22] formalism and use the term *irreducible vectors* or *irreducible features* to refer to the vectors in the representation space of irreps.

For the special orthogonal group $SO(3)$, it is known that every irreps are classified according to their angular frequency $l \in \{0, 1, 2, \dots\}$, a non-negative integer number also referred to as the *type*, or *spin*. It is known that any type- l , or spin- l representations are equivalent representations of the *real Wigner D-matrix* of degree l , denoted as $\mathbf{D}_l(R) : SO(3) \rightarrow \mathbb{R}^{(2l+1) \times (2l+1)}$. We refer to the irreducible vectors of $\mathbf{D}_l(R)$ as *type- l* , or *spin- l vectors*. Type-0 vectors are one-dimensional scalars that are invariant to rotations such that $\mathbf{D}_0(R) = 1$. On the other hand, type-1 vectors are typical 3-dimensional Euclidean vectors that are rotated by the rotation matrix R . In this paper, we follow the convention of E3NN [22] and use the x - y - z basis in which $\mathbf{D}_1(R) = R$. Note that $\mathbf{D}_0(R) = 1$ and $\mathbf{D}_1(R) = R$ have the angular frequency of 0 and 1. Therefore, \mathbf{D}_0 is invariant to any rotation and \mathbf{D}_1 is identical under full 360° rotations. In general, $\mathbf{D}_l(R)$ is identical when rotated by $\theta = 2\pi/l$.

2.2 Equivariant Descriptor Fields and Bi-equivariance

An Equivariant Descriptor Field (EDF) [19] $\varphi(x|O)$ is an $SE(3)$ -equivariant² vector field on \mathbb{R}^3 generated by a point cloud $O \in \mathcal{O}$. EDFs can be reduced into the direct sum of irreducible subspaces

$$\varphi(x|O) = \bigoplus_{n=1}^N \varphi^{(n)}(x|O)$$

where $\varphi^{(n)}(x|O) : \mathbb{R}^3 \times \mathcal{O} \rightarrow \mathbb{R}^{2l_n+1}$ is an $SE(3)$ -equivariant² type- l_n vector field generated by O . An EDF $\varphi(x|O)$ is transformed by $\Delta g = (\Delta p, \Delta R) \in SE(3)$, $\Delta p \in \mathbb{R}^3$, $\Delta R \in SO(3)$ as

$$\varphi(\Delta g x | \Delta g \cdot O) = \mathbf{D}(\Delta R) \varphi(x|O) \quad \forall \Delta g = (\Delta p, \Delta R) \in SE(3) \quad (2)$$

where $\mathbf{D}(R)$ is the block-diagonal matrix whose sub-matrices are Wigner D-matrices $\{\mathbf{D}_{l_n}(R)\}_{n=1}^N$. Ryu et al. [19] proposed to use EDFs to construct a bi-equivariant energy-based model for robotic object rearrangement tasks. We provide more explanations on bi-equivariance in Appendix A.

2.3 Brownian Diffusion on the $SE(3)$ Manifold

Let $g_t \in SE(3)$ be generated by diffusing $g_0 \in SE(3)$ for time t . The Brownian diffusion process is defined by the following Lie group stochastic differential equation (SDE)

$$g_{t+dt} = g_t \exp [dW] \quad (3)$$

²More precisely, it is $SO(3)$ -equivariant and translation-invariant, forming a subset of $SE(3)$ -equivariance.

where dW is the standard Wiener process on the Lie algebra $\mathfrak{se}(3)$, which is the 6-dimensional vector space that serves as the tangent space at the identity of $SE(3)$. The Brownian diffusion kernel $P_{t|0}(g_t|g_0) = \mathcal{B}_t(g_0^{-1}g_t)$ corresponding to the SDE in Equation (3) can be decomposed into rotational and translational parts [23, 24], i.e.,

$$\mathcal{B}_t(g) = \mathcal{N}(\mathbf{p}; \boldsymbol{\mu} = \mathbf{0}, \Sigma = tI) \mathcal{IG}_{SO(3)}(R; \epsilon = t/2) \quad (4)$$

$$\mathcal{IG}_{SO(3)}(R; \epsilon) = \left[\sum_{l=0}^{\infty} (2l+1) e^{-\epsilon l(l+1)} \frac{\sin((2l+1)\theta/2)}{\sin \theta/2} \right] \quad (5)$$

where \mathcal{N} is the normal distribution on \mathbb{R}^3 , $\mathcal{IG}_{SO(3)}$ is the isotropic Gaussian on $SO(3)$ [25–28], $g = (\mathbf{p}, R) \in SE(3)$, $\mathbf{p} \in \mathbb{R}^3$, $R \in SO(3)$, and θ is the rotation angle of $SO(3)$ in the axis-angle parameterization. R can be sampled from $\mathcal{IG}_{SO(3)}$ with the following procedure [27, 19, 28]. First, the rotation axis is sampled uniformly from the unit sphere S^2 . Next, θ is sampled using the inverse-CDF method, ranging from $\theta = 0$ to π . When calculating the cumulative distribution function (CDF), Equation (5) must be multiplied by $(1 - \cos \theta)/\pi$. This is because the invariant volume element of $SO(3)$ is $dR = (1 - \cos \theta)/\pi d\theta dS^2$ in the axis-angle parameterization.

2.4 Annealed Langevin Markov Chain Monte Carlo on the SE(3) Manifold

Let $dP_0(g) = P_0(g)dg$ be a distribution on $SE(3)$ where $P_0(g)$ is the invariant probability distribution function (PDF). The *Langevin dynamics* for $dP_0(g)$ on $SE(3)$ is defined as follows [29, 30]:

$$g_{\tau+d\tau} = g_\tau \exp \left[\frac{1}{2} \nabla \log P_0(g) d\tau + dW \right]$$

where the i -th component of ∇ is the *Lie derivative* [30] of $SE(3)$ along the i -th basis of the $\mathfrak{se}(3)$ Lie algebra. A Lie derivative $\mathcal{L}_{\mathcal{V}}$ along $\mathcal{V} \in \mathfrak{se}(3)$ acts on a differentiable function $f(g)$ on $SE(3)$ as

$$\mathcal{L}_{\mathcal{V}} f(g) = \left. \frac{d}{d\epsilon} \right|_{\epsilon=0} f(g \exp [\epsilon \mathcal{V}])$$

For brevity, we denote the Lie derivative along the i -th basis $\hat{\mathbf{e}}_i \in \mathfrak{se}(3)$ as \mathcal{L}_i instead of $\mathcal{L}_{\hat{\mathbf{e}}_i}$ such that

$$\nabla f(g) = \sum_{i=1}^6 \mathcal{L}_i f(g) \hat{\mathbf{e}}_i.$$

We denote the time for the Langevin dynamics as τ , as we will reserve the notation t for the diffusion time. It is known that under mild assumptions, this process converges to $P_0(g)$ as $\tau \rightarrow \infty$ regardless of the initial distribution. Therefore, one may sample from $P_0(g)$ with Langevin dynamics if the *score function* $s(g) = \nabla \log P_0(g)$ is known.

However, it is known to be difficult and unstable to train and sample with the score function for a sparse distribution [31, 32]. To address this issue, *Annealed Langevin Markov Chain Monte Carlo* [31, 7] method leverages the score of the diffused marginal P_t instead of P_0 . A diffused marginal $P_t(g)$ for a diffusion kernel $P_{t|0}(g|g_0)$ is defined on the $SE(3)$ manifold as

$$P_t(g) = \int_{g_0 \in SE(3)} dg_0 P_{t|0}(g|g_0) P_0(g_0) \quad (6)$$

Annealed Langevin MCMC on the $SE(3)$ manifold is defined as follows [7, 23, 24, 33, 34, 28]:

$$g_{\tau+d\tau} = g_\tau \exp \left[\frac{1}{2} \nabla \log P_{t(\tau)}(g) d\tau + dW \right] \quad (7)$$

where $t(\tau)$ is the diffusion time scheduling, which is gradually annealed to zero as $\tau \rightarrow \infty$, such that $t(\tau = \infty) = 0$. Assuming the ergodicity of Langevin dynamics, this process will converge to $P_0(g)$ regardless of the initial distribution if it is annealed sufficiently slowly and $\lim_{t \rightarrow 0} P_t = P_0$.

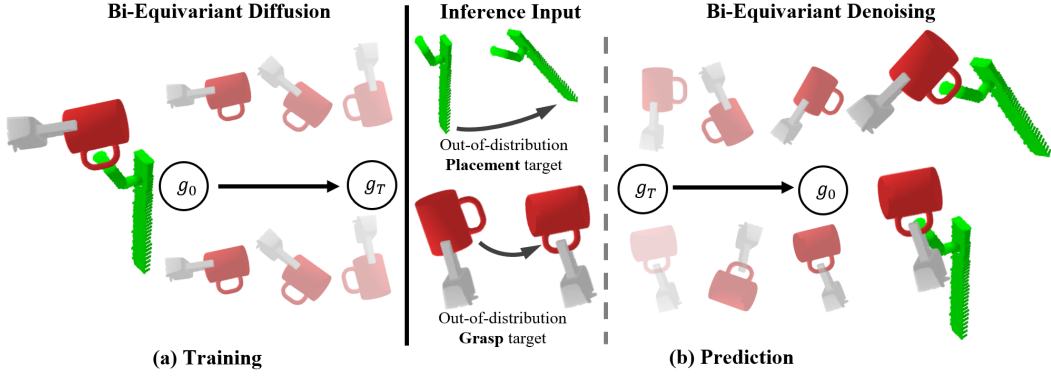


Figure 1: **Overview of Diffusion-EDFs.** (a) The target end-effector pose g_0 is diffused in a bi-equivariant manner. (b) The end-effector pose is sampled from the policy by denoising with learned bi-equivariant score function. Due to the bi-equivariance, the trained policy can be effectively generalized to unseen configurations in the observation of the scene and the grasp.

3 Bi-equivariant Score Matching on the $SE(3)$ Manifold

3.1 Problem Formulation

Let the target policy distribution³ be $P_0(g_0|O^{(s)}, O^{(b)})$, where $g_0 \in SE(3)$ is the target end-effector pose, and $O^{(s)}$ and $O^{(b)}$ are the observed point clouds of the scene and the grasped object, respectively. Following Ryu et al. [19], we model this target policy to be bi-equivariant (see Appendix A):

$$P_0(\Delta g | \Delta g \cdot O^{(s)}, O^{(b)}) = P_0(g | O^{(s)}, O^{(b)}) = P_0(g \Delta g^{-1} | O^{(s)}, \Delta g \cdot O^{(b)}) \quad (8)$$

Now let $g_t \in SE(3)$ be the samples that are noised from g_0 by some diffusion process, where t denotes the diffusion time. A detailed explanation of this diffusion process will be deferred to a subsequent section. Our goal is to train a model that denoises g_t , which is sampled from the diffused marginal distribution $P_t(g_t | O^{(s)}, O^{(b)})$, into a denoised sample g , which follows the target distribution $P_0(g | O^{(s)}, O^{(b)})$. This can be achieved with Annealed Langevin MCMC if the score function (see Section 2.4) of the diffused marginal distribution is known. The score function $s(g | O^{(s)}, O^{(b)}) : SE(3) \rightarrow \mathfrak{se}(3)$ for a probability distribution $P(g | O^{(s)}, O^{(b)})$ is defined as

$$s(g | O^{(s)}, O^{(b)}) = \nabla \log P(g | O^{(s)}, O^{(b)}) = \sum_{i=1}^6 \mathcal{L}_i \log P(g | O^{(s)}, O^{(b)}) \hat{e}_i. \quad (9)$$

3.2 Bi-equivariant Score Function

For a bi-equivariant distribution, the score function satisfies special equivariance conditions that can be exploited for our model design.

Proposition 1. *Let a probability distribution $P(g | O^{(s)}, O^{(b)})$ be bi-equivariant such that it satisfies Equation (8). The score function then satisfies the following two equivariance conditions:*

$$s(\Delta g | \Delta g \cdot O^{(s)}, O^{(b)}) = s(g | O^{(s)}, O^{(b)}) \quad \forall \Delta g \in SE(3) \quad (10)$$

$$s(g \Delta g^{-1} | O^{(s)}, \Delta g \cdot O^{(b)}) = [\text{Ad}_{\Delta g}]^{-T} s(g | O^{(s)}, O^{(b)}) \quad \forall \Delta g \in SE(3) \quad (11)$$

Ad_g is the *adjoint representation* [30, 35, 37] of $SE(3)$ with $g = (\mathbf{p}, R)$, $\mathbf{p} \in \mathbb{R}^3$, and $R \in SO(3)$

$$\text{Ad}_g = \begin{bmatrix} R & [\mathbf{p}]^\wedge R \\ \emptyset & R \end{bmatrix} \quad (12)$$

³For notational simplicity, we do not distinguish the probability distribution $dP = P dg$ from the probability distribution function (PDF) P where dg denotes the bi-invariant volume form [30, 35, 36] on $SE(3)$.

where $[\mathbf{p}]^\wedge$ denotes the skew-symmetric 3×3 matrix of \mathbf{p} . We follow the notation from Murray et al. [35] and place the translational part in the upper rows. See Appendix C.1 for the proof of Proposition 1. We refer to Equation (10) as the *left invariance* of the score, since Δg comes to the left side of g , and the score remains invariant. Likewise, we refer to Equation (11) as the *right equivariance* of the score, as the inverse of Δg comes to the right side of g , and the score is adjoint-transformed accordingly.

3.3 Bi-equivariant Diffusion Process

Let the point cloud conditioned diffusion kernel be $P_{t|0}(g|g_0, O^{(s)}, O^{(b)})$ such that the diffused marginal $P_t(g|O^{(s)}, O^{(b)})$ for the initial target distribution $P_0(g|O^{(s)}, O^{(b)})$ is defined as follows:

$$P_t(g|O^{(s)}, O^{(b)}) = \int_{g_0 \in SE(3)} dg_0 P_{t|0}(g|g_0, O^{(s)}, O^{(b)}) P_0(g_0|O^{(s)}, O^{(b)}) \quad (13)$$

If the diffused marginal $P_t(g|O^{(s)}, O^{(b)})$ is bi-equivariant, one may leverage the equivariance property of the target score function $\nabla \log P_t(g|O^{(s)}, O^{(b)})$ to design the score model.

Definition 1. A bi-equivariant diffusion kernel $P_{t|0}(g|g_0, O^{(s)}, O^{(b)})$ is a square-integrable kernel that satisfies the following equations for all $\Delta g \in SE(3)$, except on a set of measure zero:

$$P_{t|0}(g|g_0, O^{(s)}, O^{(b)}) = P_{t|0}(\Delta g g|\Delta g g_0, \Delta g \cdot O^{(s)}, O^{(b)}) \quad (14)$$

$$= P_{t|0}(g \Delta g^{-1}|g_0 \Delta g^{-1}, O^{(s)}, \Delta g \cdot O^{(b)}) \quad (15)$$

Proposition 2. The diffused marginal P_t is guaranteed to be bi-equivariant for all bi-equivariant initial distribution P_0 if and only if the diffusion kernel $P_{t|0}$ is bi-equivariant.

See Appendix C.2 for the proof of Proposition 2. However, the Brownian diffusion kernel $P_{t|0}(g|g_0) = \mathcal{B}_t(g_0^{-1}g)$ in Equation (4) is left invariant⁴ but not right invariant⁴, that is

$$P_{t|0}(\Delta g g|\Delta g g_0) = P_{t|0}(g|g_0), \quad P_{t|0}(g \Delta g^{-1}|g_0 \Delta g^{-1}) \neq P_{t|0}(g|g_0) \quad \forall \Delta g \in SE(3)$$

In fact, there exist no square-integrable kernel on $SE(3)$ that is bi-invariant⁴ (see Appendix C.3). Therefore, we propose to let the diffusion kernel be at least dependent on either $O^{(s)}$ or $O^{(b)}$ to absorb the left or right group action of Δg . For generality, we keep both $O^{(s)}$ and $O^{(b)}$ in the following.

While there may be numerous ways to implement such bi-equivariant diffusion kernels, we use a diffusion kernel with an equivariant *diffusion frame selection mechanism* $P_{ref}(g_{ref}|g_0^{-1} \cdot O^{(s)}, O^{(b)})$

$$P_{t|0}(g|g_0, O^{(s)}, O^{(b)}) = \int_{g_{ref} \in SE(3)} dg_{ref} P_{ref}(g_{ref}|g_0^{-1} \cdot O^{(s)}, O^{(b)}) K_t(g_{ref}^{-1} g_0^{-1} g g_{ref}) \quad (16)$$

where $K_t(g_0^{-1}g)$ is any left invariant kernel⁵ and $g_{ref} \in SE(3)$ is the reference frame of the diffusion in the end-effector frame. The diffusion procedure is as follows:

- D1. A target pose $g_0 \sim P_0(g_0|O^{(s)}, O^{(b)})$ is sampled from the demonstration policy.
- D2. A diffusion reference frame $g_{ref} \sim P_{ref}(g_{ref}|g_0^{-1} \cdot O^{(s)}, O^{(b)})$ is sampled from the diffusion frame selection mechanism.
- D3. A diffusion displacement $\Delta g_{t|0} \sim K_t(\Delta g_{t|0})$ is sampled from K_t in Equation (16).
- D4. The sampled $\Delta g_{t|0}$ is applied to g_0 within the reference frame of diffusion g_{ref} such that $g_t = g_0 g_{ref} \Delta g_{t|0} g_{ref}^{-1}$ where $g_t \sim P_t$ is the diffused end-effector pose.

Proposition 3. The diffusion kernel in Equation (16) is bi-equivariant if the diffusion frame selection mechanism $P_{ref}(g_{ref}|g_0^{-1} \cdot O^{(s)}, O^{(b)})$ satisfies the following property:

$$P_{ref}(g_{ref}|g_0^{-1} \cdot O^{(s)}, O^{(b)}) = P_{ref}(\Delta g g_{ref}|(\Delta g g_0^{-1}) \cdot O^{(s)}, \Delta g \cdot O^{(b)}) \quad (17)$$

⁴ We use the term *invariance* instead of equivariance since the kernel is neither conditioned by $O^{(s)}$ nor $O^{(b)}$.

⁵ Note that any left invariant kernel $K_t(g, g_0)$ can be written as $K_t(g_0^{-1}g)$ (see Appendix C.3).

See Appendix C.4 for the proof. In practice, however, the orientational part of the frame selection mechanism may be difficult to implement. Remarkably, for the specific case in which K_t is the Brownian diffusion kernel \mathcal{B}_t , only the translation part of the frame selection is required for Equation (16) to be bi-equivariant. For example, consider the following frame selection mechanism

$$P_{ref}(g_{ref}|g_0^{-1} \cdot O^{(s)}, O^{(b)}) = P_{origin}(\mathbf{p}_{ref}|g_0^{-1} \cdot O^{(s)}, O^{(b)}) \delta_{SO(3)}(R_{ref}) \quad (18)$$

where $\delta_{SO(3)}$ is the Dirac delta on $SO(3)$ such that the orientation part of g_{ref} is always same as the identity, and $P_{origin}(\mathbf{p}_{ref}|g_0^{-1} \cdot O^{(s)}, O^{(b)})$ is the *diffusion origin selection mechanism*.

Proposition 4. *The diffusion kernel $P_{t|0}$ in Equation (16) with the frame selection mechanism P_{ref} in Equation (18) is bi-equivariant if K_t in Equation (16) is the Brownian diffusion kernel⁶ \mathcal{B}_t and the origin selection mechanism P_{origin} in Equation (18) is equivariant such that*

$$P_{origin}(\mathbf{p}_{ref}|g_0^{-1} \cdot O^{(s)}, O^{(b)}) = P_{origin}(\Delta g \mathbf{p}_{ref} | (\Delta g g_0^{-1}) \cdot O^{(s)}, \Delta g \cdot O^{(b)}) \quad (19)$$

We provide the proof in Appendix C.5. A concrete realization of such equivariant diffusion origin selection mechanism $P_{origin}(\mathbf{p}_{ref}|g_0^{-1} \cdot O^{(s)}, O^{(b)})$ is discussed in Section 4.1.

3.4 Score Matching Objectives

In contrast to Song and Ermon [31], Urain et al. [7], our diffusion kernel $P_{t|0}(g|g_0, O^{(s)}, O^{(b)})$ in Equation (16) is not the Brownian kernel. Still, the following mean squared error (MSE) loss can be used to train our score model $s_t(g|O^{(s)}, O^{(b)})$ without requiring the integration of Equation (16):

$$\mathcal{J}_t = \mathbb{E}_{g, g_0, g_{ref}, O^{(s)}, O^{(b)}} \left[\frac{1}{2} \left\| s_t(g|O^{(s)}, O^{(b)}) - \nabla \log K_t(g_{ref}^{-1} g_0^{-1} g g_{ref}) \right\|^2 \right] \quad (20)$$

where $g_0 \sim P_0(g_0|O^{(s)}, O^{(b)})$, $g_{ref} \sim P_{ref}(g_{ref}|g_0^{-1} \cdot O^{(s)}, O^{(b)})$, and $g \sim P_{t|0}(g|g_0, O^{(s)}, O^{(b)})$. We optimize \mathcal{J}_t for sampled reference frame g_{ref} and diffusion time t . The minimizer of \mathcal{J}_t is neither $\nabla \log K_t$ nor $\nabla \log P_{t|0}$ but the score function of the diffused marginal $\nabla \log P_t$, that is

$$\arg \min_{s_t(g|O^{(s)}, O^{(b)})} \mathcal{J}_t = s_t^*(g|O^{(s)}, O^{(b)}) = \nabla \log P_t(g|O^{(s)}, O^{(b)}) \quad (21)$$

Although Equation (21) is a straightforward adaptation of the MSE minimizer formula [31], we still provide the derivation in Appendix C.6 for completeness. In practice, we use the Brownian diffusion kernel \mathcal{B}_t for K_t to exploit Proposition 4. Therefore, training with Equation (20) requires the computation of $\nabla \log \mathcal{B}_t(g_{ref}^{-1} g_0^{-1} g g_{ref})$. While autograd packages are commonly used for the calculation of Lie derivatives [27, 19, 28, 7, 24, 23], we provide the explicit form in Appendix B.

3.5 Bi-equivariant Score Model

To model the left invariance and the right equivariance of the score function as in Equation (10) and Equation (11), we propose the following score model on $SE(3)$:

$$s_t(g|O^{(s)}, O^{(b)}) = s_{\nu;t}(g|O^{(s)}, O^{(b)}) \oplus s_{\omega;t}(g|O^{(s)}, O^{(b)}) \quad (22)$$

$$s_{\nu;t}(g|O^{(s)}, O^{(b)}) = \int_{\mathbb{R}^3} d^3 \mathbf{x} \rho_{\nu;t}(\mathbf{x}|O^{(b)}) \tilde{s}_{\nu;t}(g, \mathbf{x}|O^{(s)}, O^{(b)}) \quad (23)$$

$$\begin{aligned} s_{\omega;t}(g|O^{(s)}, O^{(b)}) &= \underbrace{\int_{\mathbb{R}^3} d^3 \mathbf{x} \rho_{\nu;t}(\mathbf{x}|O^{(b)}) \mathbf{x} \times \tilde{s}_{\nu;t}(g, \mathbf{x}|O^{(s)}, O^{(b)})}_{\text{Orbital term}} \\ &+ \underbrace{\int_{\mathbb{R}^3} d^3 \mathbf{x} \rho_{\omega;t}(\mathbf{x}|O^{(b)}) \tilde{s}_{\omega;t}(g, \mathbf{x}|O^{(s)}, O^{(b)})}_{\text{Spin term}} \end{aligned} \quad (24)$$

where \oplus and \times denote direct sum (concatenation) and cross product, respectively. We denote the translational part with subscript ν and rotational part with subscript ω . In Equation (22), we decompose the score model $s_t(\cdot|O^{(s)}, O^{(b)}) : SE(3) \rightarrow \mathfrak{se}(3) \cong \mathbb{R}^6$ into the translational score model

⁶In fact, any left-invariant kernel that is also right-invariant to rotation as in Equation (40) can be used.

$s_{\nu;t}(\cdot|O^{(s)}, O^{(b)}) : SE(3) \rightarrow \mathbb{R}^3$ and the rotational score model $s_{\omega;t}(\cdot|O^{(s)}, O^{(b)}) : SE(3) \rightarrow \mathfrak{so}(3) \cong \mathbb{R}^3$. Next, we model these translational and rotational score model using two different types of equivariant fields: 1) the equivariant density field $\rho_{\square;t}(\cdot|O^{(b)}) : \mathbb{R}^3 \rightarrow \mathbb{R}_{\geq 0}$, and 2) the time-conditioned score field $\tilde{s}_{\square;t}(\cdot|O^{(s)}, O^{(b)}) : SE(3) \times \mathbb{R}^3 \rightarrow \mathbb{R}^3$, where \square is either ω or ν .

Proposition 5. *The score model in Equation (22) is left invariant and right equivariant if for $\square = \omega, \nu$ the density and score fields satisfy the following equivariance conditions*

$$\rho_{\square;t}(\Delta g \mathbf{x} | \Delta g \cdot O^{(b)}) = \rho_{\square;t}(\mathbf{x} | O^{(b)}) \quad \forall \Delta g \in SE(3) \quad (25)$$

$$\tilde{s}_{\square;t}(\Delta g \mathbf{x} | \Delta g \cdot O^{(s)}, O^{(b)}) = \tilde{s}_{\square;t}(g, \mathbf{x} | O^{(s)}, O^{(b)}) \quad \forall \Delta g \in SE(3) \quad (26)$$

$$\tilde{s}_{\square;t}(g \Delta g^{-1}, \Delta g \mathbf{x} | O^{(s)}, \Delta g \cdot O^{(b)}) = \Delta R \tilde{s}_{\square;t}(g, \mathbf{x} | O^{(s)}, O^{(b)}) \quad \forall \Delta g \in SE(3) \quad (27)$$

See Appendix C.7 for the proof. To achieve the left invariance (Equation (26)) and right equivariance (Equation (27)) of the score field, we propose using the following model with two EDFs:

$$\tilde{s}_{\square;t}(g, \mathbf{x} | O^{(s)}, O^{(b)}) = \psi_{\square;t}(\mathbf{x} | O^{(b)}) \otimes_{\square;t}^{(\rightarrow 1)} \mathbf{D}(R^{-1}) \varphi_{\square;t}(g \mathbf{x} | O^{(s)}) \quad (28)$$

where $\varphi_{\square;t}$ and $\psi_{\square;t}$ are two different EDFs that respectively encode the point clouds $O^{(s)}$ and $O^{(b)}$, and $\otimes_{\square;t}^{(\rightarrow 1)}$ is the time-conditioned equivariant low-rank tensor product [38, 39] that maps the highly over-parametrized equivariant descriptors into a type-1 vector.

Proposition 6. *The score field model in Equation (28) satisfies Equation (26) and Equation (27).*

We provide the proof of Proposition 6 in Appendix C.8. Note that the resulting score field model $\tilde{s}_{\square;t}(g, \mathbf{x} | O^{(s)}, O^{(b)})$ can be considered as the type-1 generalization to the energy function of Ryu et al. [19], which is a type-0 (rotation invariant scalar) function.

4 Implementation

In this section, we first provide the specific implementation of the bi-equivariant diffusion frame selection mechanism, which was postponed in Section 3.3. We thereafter propose the novel architectures of EDFs and density fields proposed in Section 3.5.

4.1 Bi-equivariant Diffusion Frame Selection with Contact Heuristics

Real-world objects may be decomposed into local sub-geometries. For the most of the cases, some sub-geometries are more significant than others in terms of deciding the target end-effector pose. Therefore, a desirable model should exhibit equivariance to important local sub-geometries instead of the global geometry. Such importance of incorporating locality in equivariant methods has recently been reported in various works [15, 19, 20, 40, 41].

To capture such important sub-geometries, we take into account the local contact points. It is highly likely that sub-geometries with rich contact are more important than those without any contact. A straightforawd way to inject this inductive bias is to *select the reference frame of diffusion near the contact points*. We find that this strategy enables our models to identify and pay more attention to such contact-rich and relevant sub-geometries without explicit supervision. Note that it only suffices to sample the origin of diffusion, due to Proposition 4.

Let $n_r(\mathbf{x}, O)$ be the number of points in a point cloud O that is within a contact radius r from a point $\mathbf{x} \in \mathbb{R}^3$. We use the following diffusion origin selection mechanism with r as a hyperparameter.

$$P_{\text{origin}}(\mathbf{p}_{\text{ref}} | g_0^{-1} \cdot O^{(s)}, O^{(b)}) \propto \begin{cases} n_r(\mathbf{p}_{\text{ref}}, g_0^{-1} \cdot O^{(s)}) & \text{if } \mathbf{p}_{\text{ref}} \in O^{(b)} \\ 0 & \text{else} \end{cases} \quad (29)$$

For each point in $O^{(b)}$, we first calculate the number of neighboring points in $g_0^{-1} \cdot O^{(s)}$. We then randomly sample a point from $O^{(b)}$ as the origin of diffusion with the probability proportional to the number of neighbors. Although this specific frame origin selection mechanism allows tractable integration of Equation (16), we efficiently approximate it by using the loss function in Equation (20) with a minibatch of a few \mathbf{p}_{ref} . Note that this approach is more general and can be applied for an arbitrary frame selection mechanism whose integration of Equation (16) is intractable.

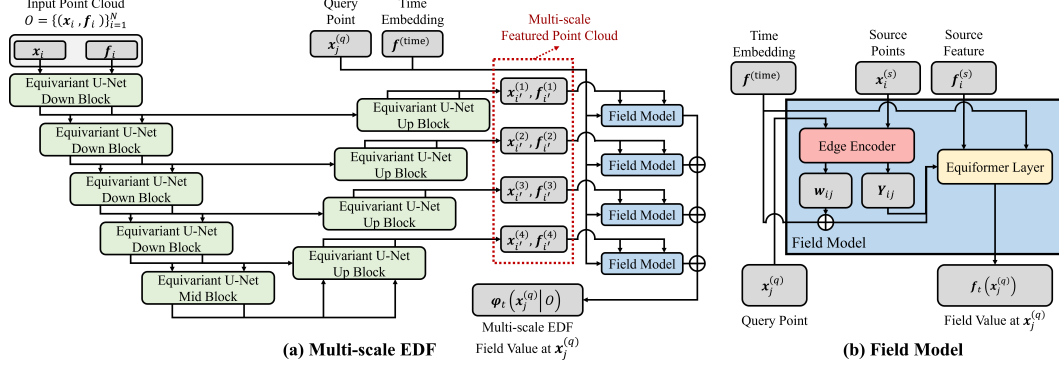


Figure 2: **Architecture of multiscale EDF.** Our multiscale EDF model is composed of a feature extracting part and a field model part. See Figure 3 for details on each module in the architecture. **(a)** The feature extractor encodes the input point cloud into multiscale featured point clouds. We use an U-Net-like GNN architecture for the feature extractor part. **(b)** The encoded multiscale point clouds are passed into the field model part along with the query point and optional time embedding. The field model part outputs the time-conditioned EDF field value at the query point. We simply add the field value for each scale to obtain the multiscale EDF field value, which is used to infer the score.

4.2 Architecture of Equivariant Descriptor Fields

In practice, we use shared EDFs and density fields for $\square = \omega$ and ν to save on computation. Therefore, the equivariant low-rank tensor product $\otimes_{\square; t}^{(\rightarrow 1)}$ is the only operation that distinguishes the linear score (ν) from the angular score (ω). We also drop the time dependence for the density field (ρ) and the grasp EDF (ψ) because evaluating them for every diffusion timestep t is inefficient. Hence, we denote these models as $\varphi_t(\mathbf{x}|O^{(s)})$, $\psi(\mathbf{x}|O^{(b)})$, $\rho(\mathbf{x}|O^{(b)})$. Consequently, time dependence is only left for the tensor product $\otimes_{\square; t}^{(\rightarrow 1)}$ and the scene EDF $\varphi_t(\mathbf{x}|O^{(s)})$.

Similar to Ryu et al. [19], Chatzipantazis et al. [40], we separate the EDFs into a feature extractor and a field model (see Figure 2). The feature extractor is a deep $SE(3)$ -equivariant GNN based encoder that is run only once in the beginning of the denoising process. Note that the EDFs used in our score models must have significantly wide receptive fields for denoising diffusion, such that they can cover the whole scene while keeping the local high-frequency details. Therefore, a hierarchical modeling is required to effectively capture this multiscale representations. For this reason, we propose an UNet-like architecture based on Equiformer [42] for the feature extractor, which is analogous to diffusion models for image generation. However, the original Equiformer assumes source and destination points to be identical, which cannot be met in our application. To address this discrepancy, we slightly modify the architecture to accommodate skip connections between source and destination points. We use the *Farthest Point Sampling* (FPS) algorithm [43] for the point pooling.

The encoded multiscale feature points from the feature extractor are then passed into the much shallower field model for each denoising timestep. The field model is also an Equiformer-based $SE(3)$ -equivariant GNN but is much shallower and hence much faster than the feature extractor. We find that only a single layer is enough for the field model. While it is possible to stack multiple layers for the field model as Chatzipantazis et al. [40], we find this does not improve and even damages the accuracy of the estimated score in our case, presumably due to the limited number of training data. The overview of the modules in our architecture is illustrated in Figure 3.

4.3 Score Model

Density Field. We use the weighted query points model of Ryu et al. [19] for $\rho(\mathbf{x}|O)$

$$\mathbf{x}_n^{(q)} = \mathbf{q}_n(O^{(b)}) \quad (30)$$

$$\rho(\mathbf{x}|O^{(b)}) = \sum_{n=1}^{N_q} w(\mathbf{x}|O^{(b)}) \delta^{(3)}(\mathbf{x} - \mathbf{x}_n^{(q)}) \quad (31)$$

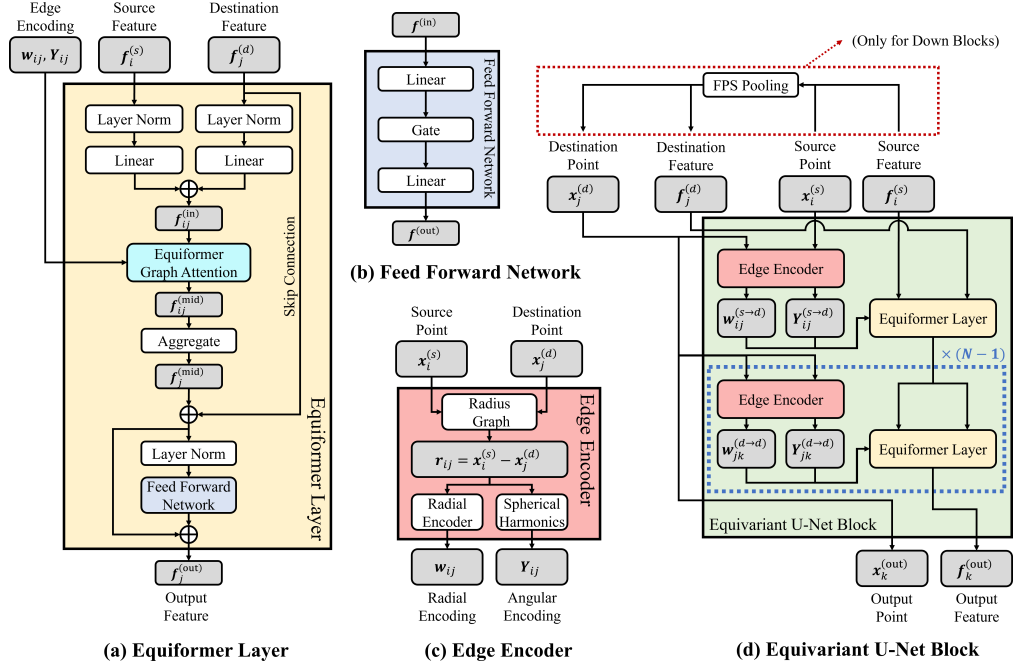


Figure 3: **Overview of modules used in multiscale EDF.** (a) We employ Equiformer [42] to achieve $SE(3)$ -equivariance in our model. (b) We use an equivariant feed forward network with gate activation from Equiformer. (c) We use radius graph to construct graph from points. Graph edge length and orientation are respectively encoded by a radial encoder and spherical harmonics [38, 39, 42]. (d) Multiple equiformer layers are stacked and form the equivariant U-Net Block. FPS pooling is used in downward blocks to obtain destination points of larger scale.

where $q_n(O^{(b)}) \in \mathbb{R}^3$ is the n -th *query point function* and $w(\cdot|O^{(b)}) : \mathbb{R}^3 \rightarrow \mathbb{R}_{\geq 0}$ is the *query weight field* that assigns non-negative weights to each query points. The query point function and query weight field are $SE(3)$ -equivariant such that

$$\begin{aligned} q_n(\Delta g \cdot O^{(b)}) &= \Delta g \cdot q_n(O^{(b)}) & \forall \Delta g \in SE(3) \\ w(\Delta g \cdot \mathbf{x} | \Delta g \cdot O^{(b)}) &= w(\mathbf{x} | O^{(b)}) & \forall \Delta g \in SE(3) \end{aligned}$$

We use FPS algorithm for the query point function $q_n(O)$. Although it is not strictly deterministic, we observe negligible impact from this stochasticity. For the implementation of the query weight field $w(\mathbf{x}|O)$, we use an EDF with a single scalar output.

Non-dimensionalization. We assume that the output of the score field model in Equation (28) is a dimensionless quantity. Therefore, we obtain the dimensionful score by taking

$$\tilde{s}_{\nu;t} \rightarrow \frac{1}{L\sqrt{t}} \tilde{s}_{\nu;t}, \quad \tilde{s}_{\omega;t} \rightarrow \frac{1}{\sqrt{t}} \tilde{s}_{\omega;t}$$

where L is the characteristic length scale unit. The reason for dividing $1/\sqrt{t}$ is because the norm of the target score tend to scale with $O(1/\sqrt{t})$. Likewise, we divide the linear score field by L because score field is a gradient and thus scales reciprocally to the characteristic length scale.

Score Function. In conclusion, Equation (23) and Equation (24) become tractable summation forms

$$\begin{aligned} s_{\nu;t}(g|O^{(s)}, O^{(b)}) &= \frac{1}{L\sqrt{t}} \sum_{n=1}^{N_q} w(\mathbf{x}_n^{(q)}|O^{(b)}) \left[\psi(\mathbf{x}_n^{(q)}|O^{(b)}) \otimes_{\nu;t}^{(\rightarrow 1)} \mathbf{D}(R^{-1}) \varphi_t(g \mathbf{x}_n^{(q)}|O^{(s)}) \right] \\ s_{\omega;t}(g|O^{(s)}, O^{(b)}) &= \frac{1}{\sqrt{t}} \sum_{n=1}^{N_q} w(\mathbf{x}_n^{(q)}|O^{(b)}) \frac{\mathbf{x}_n^{(q)}}{L} \times \left[\psi(\mathbf{x}_n^{(q)}|O^{(b)}) \otimes_{\nu;t}^{(\rightarrow 1)} \mathbf{D}(R^{-1}) \varphi_t(g \mathbf{x}_n^{(q)}|O^{(s)}) \right] \\ &+ \frac{1}{\sqrt{t}} \sum_{n=1}^{N_q} w(\mathbf{x}_n^{(q)}|O^{(b)}) \left[\psi(\mathbf{x}_n^{(q)}|O^{(b)}) \otimes_{\omega;t}^{(\rightarrow 1)} \mathbf{D}(R^{-1}) \varphi_t(g \mathbf{x}_n^{(q)}|O^{(s)}) \right] \end{aligned}$$

4.4 Sampling with Annealed Langevin Dynamics

For denoising, we use the trained scores for the annealed Langevin MCMC (see section 2.4). The annealed Langevin MCMC for our trained score model on $SE(3)$ is written as follows:

$$g_{\tau+d\tau} = g_\tau \exp \left[\frac{1}{2} \mathbf{s}_{t(\tau)}(g_\tau | O^{(s)}, O^{(b)}) d\tau + dW \right] \quad (32)$$

This SDE can be discretized using the forward Euler-Maruyama method such that

$$g_{n+1} = g_n \exp \left[\frac{1}{2} \mathbf{s}_{t[n]}(g_n | O^{(s)}, O^{(b)}) \alpha[n] + \sqrt{\alpha[n]} \mathbf{z}_n \right], \quad \mathbf{z}_n \sim \mathcal{N}(\mathbf{0}, I) \quad (33)$$

where $t[n]$ and $\alpha[n]$ are respectively the diffusion time and Langevin step size, both of which are scheduled according to the step count n . A commonly used scheduling scheme is taking $\alpha[n] \propto t[n]$ with either a linear or log-linear $t[n]$ schedule [31, 44, 7]. However, the convergence is very slow with this scheduling. Therefore, we use $\alpha[n] \propto t[n]^{k_1}$ schedule with a hyperparameter $k_1 < 1$. To suppress the instability caused by large step sizes when t is small, we also gradually lower the *temperature*⁷ of the process. This can be done by using $\sqrt{\alpha[n]T[n]}\mathbf{z}_n$ instead of $\sqrt{\alpha[n]}\mathbf{z}_n$ for the noise term with the temperature schedule $T[n] = t[n]^{k_2}$, where $k_2 \geq 0$ is another hyperparameter. Intuitively, this makes the sampling process to smoothly transition into a simple gradient descent optimization as $t[n] \rightarrow 0$, and hence $T[n] \rightarrow 0$. We empirically found that this strategy significantly improves the convergence time without compromising the accuracy and diversity of the sampled poses. The resulting proposed sampling algorithm with a small number ϵ is

$$g_{n+1} = g_n \exp \left[\frac{\epsilon}{2} \mathbf{s}_{t[n]}(g_n | O^{(s)}, O^{(b)}) t[n]^{k_1} + t[n]^{\frac{k_1+k_2}{2}} \mathbf{z}_n \right], \quad \mathbf{z}_n \sim \mathcal{N}(\mathbf{0}, I) \quad (34)$$

We use $k_1 = 0.5$ and $k_2 = 1.0$ for the step size and temperature scheduling. For the diffusion time $t[n]$, we use piecewise linear scheduling. For example, we linearly schedule the diffusion time for $t = 1$ to $t = 0.1$ and then with $t = 0.1$ to $t = 0.01$. Similar to diffusion-based image generation models, we separate a low-resolution model and high-resolution model instead of using a single model. We use the low-resolution model for higher t and the high-resolution model for lower t .

5 Experimental Results

We evaluate the data-efficiency, generalizability, and robustness of our methods following a similar evaluation protocol as in Simeonov et al. [13, 14], Ryu et al. [19], Biza et al. [45]. In particular, we evaluate the pick-and-place success rate for two different object categories: mugs and bottles, in which a mug should be placed on a rack and a bottle on a tray. All the models are trained with 10 task demonstrations (two demonstrations for five different object instances), performed by humans, for each pick and place task. Each demonstration is a tuple of $(O^{(s)}, O^{(b)}, g_0)$ where $O^{(s)}$ and $O^{(b)}$ are the point cloud observation of the scene and grasp, and g_0 is the target end-effector pose.

We assess the generalizability and robustness of the methods under four previously unseen scenarios: 1) previously unseen object instances (within the trained object category), 2) previously unseen object poses, 3) previously unseen clutters of distracting objects, 4) and all of the three combined. Evaluations are performed in a simulated environment with SAPIEN [46] with nine ceiling-mounted depth cameras and a Franka Panda robot. To minimize the influence of the quality of the motion planning, we turn off the collision between the environment and the robot during moving. Nonetheless, we fully simulate the grasp, because in reality, the actual grasp pose may differ from the intended pose, especially when a low-quality pose is inferred.

We compare our method (Diffusion-EDFs) against a state-of-the-art $SE(3)$ bi-equivariant method (R-NDFs [14]) and a state-of-the-art denoising diffusion-based method ($SE(3)$ -Diffusion Fields [7]). We train our models only with ten task demonstrations without resorting to any type of pre-training or object segmentation or detection pipelines. In contrast, R-NDFs and $SE(3)$ -Diffusion Fields greatly suffer when the target object is not segmented out from the scene point cloud. Therefore, we

⁷This temperature annealing should not be confused with that of the ‘annealed’ Langevin MCMC in which the diffusion time t is decreased.

Table 1: Pick-and-place success rates in various out-of-distribution settings in simulated environment.

	Mug			Bottle		
	Pick	Place	Total	Pick	Place	Total
Default (Trained Setup)						
R-NDFs [†] [14] w/ seg.	0.83	0.97	0.81	0.91	0.73	0.67
R-NDFs [†] [14] w/o seg.	0.00	0.00	0.00	0.00	0.00	0.00
SE(3)-DiffusionFields [‡] [7] w/ seg.	0.75	(n/a)	(n/a)	0.47	(n/a)	(n/a)
SE(3)-DiffusionFields [‡] [7] w/o seg.	0.11	(n/a)	(n/a)	0.01	(n/a)	(n/a)
Diffusion-EDFs* (Ours)	0.99	0.96	0.95	0.97	0.85	0.83
Previously Unseen Instances						
R-NDFs [†] [14] w/ seg.	0.73	0.70	0.51	0.90	0.87	0.79
R-NDFs [†] [14] w/o seg.	0.00	0.00	0.00	0.00	0.00	0.00
SE(3)-DiffusionFields [‡] [7] w/ seg.	0.55	(n/a)	(n/a)	0.57	(n/a)	(n/a)
SE(3)-DiffusionFields [‡] [7] w/o seg.	0.14	(n/a)	(n/a)	0.00	(n/a)	(n/a)
Diffusion-EDFs* (Ours)	0.96	0.96	0.92	0.99	0.91	0.90
Previously Unseen Poses						
R-NDFs [†] [14] w/ seg.	0.84	0.93	0.78	0.65	0.72	0.47
R-NDFs [†] [14] w/o seg.	0.00	0.00	0.00	0.00	0.00	0.00
SE(3)-DiffusionFields [‡] [7] w/ seg.	0.75	(n/a)	(n/a)	0.47	(n/a)	(n/a)
SE(3)-DiffusionFields [‡] [7] w/o seg.	0.00	(n/a)	(n/a)	0.04	(n/a)	(n/a)
Diffusion-EDFs* (Ours)	0.98	0.98	0.96	0.98	0.81	0.79
Previously Unseen Clutters[§]						
R-NDFs [†] [14] w/o seg.	0.01	0.00	0.00	0.00	0.00	0.00
SE(3)-DiffusionFields [‡] [7] w/o seg.	0.06	(n/a)	(n/a)	0.03	(n/a)	(n/a)
Diffusion-EDFs* (Ours)	0.91	1.00	0.91	0.96	0.91	0.87
Previously Unseen Instances, Poses, & Clutters[§]						
R-NDFs [†] [14] w/ seg.	0.71	0.75	0.53	0.85	0.84	0.72
R-NDFs [†] [14] w/o seg.	0.00	0.00	0.00	0.00	0.00	0.00
SE(3)-DiffusionFields [‡] [7] w/ seg.	0.58 [§]	(n/a)	(n/a)	0.59 [§]	(n/a)	(n/a)
SE(3)-DiffusionFields [‡] [7] w/o seg.	0.03 [§]	(n/a)	(n/a)	0.00 [§]	(n/a)	(n/a)
Diffusion-EDFs* (Ours)	0.89	0.89	0.79	0.98	0.89	0.87

^{*} No pre-training or segmentation pipeline is used for Diffusion-EDFs (Ours).

[†] Category specific self-supervised pre-training is used for R-NDFs.

[‡] Rotational data augmentation is applied for training SE(3)-Diffusion Fields.

[§] Models with segmented inputs are only tested for scenes without cluttered objects to guarantee the perfectness of object segmentation.

evaluate R-NDFs and *SE(3)*-Diffusion Fields both with and without object segmentation pipelines. Furthermore, to achieve reasonable success rate, R-NDFs require additional self-supervised training which require massive amount of category specific object geometry data. Therefore, we use the pre-trained weights from the original implementation of R-NDFs [14] trained with ShapeNet [47] dataset and procedurally generated object meshes. Still, we observe that R-NDFs fail to place the mug on a rack due to the discrepancy of the shape of the rack in our experiment and the pre-trained ones. Therefore, we do R-NDFs an additional favor of using the pre-trained rack instead of our rack for the evaluation. Lastly, we help *SE(3)*-Diffusion Fields by using rotational data augmentation, as they are not *SE(3)*-equivariant. The experimental results are summarized in Table 1.

Analysis. As shown in Table 1, Diffusion-EDFs consistently outperform both the *SE(3)*-equivariant baseline (R-NDFs [14]) and diffusion model baseline (*SE(3)*-DiffusionFields [7]) in almost all scenarios. Notably, the baseline models completely fail with unsegmented observations, whereas Diffusion-EDFs maintain a total success rate exceeding 80% in most scenarios.

When dealing with segmented observations, the baseline models can perform object pick/place tasks, yet their success rates remain inferior to those of Diffusion-EDFs. Remarkably, Diffusion-EDFs achieve comparable or superior performance without necessitating any form of pretraining, in contrast to R-NDFs that rely on self-supervised pretraining that requires copious amount of category-specific object geometry data. *SE(3)*-Diffusion Fields, despite being trained with rotationally augmented

data, lag significantly behind both Diffusion-EDFs and R-NDFs. This sub-par performance is likely attributed to the absence of $SE(3)$ -equivariance in the model’s architecture.

Interestingly, all three methods consistently exhibit better performance for the bottle pick-and-place task with previously unseen object instances. We find this is due to an outlier bottle instance which has much taller shape than others. The lower success rate of R-NDFs for bottles in previously unseen poses is due to the occlusion of the point cloud observations. We also find that $SE(3)$ -DiffusionFields cannot distinguish the bottom of the bottle with the top of the bottle, resulting in low success rate. We presume this is due to the artifact of the global $SO(3)$ augmentation. On the other hand, Diffusion-EDFs exhibit robustness to such partial occlusion or spurious correlation with global geometry by only attending to relevant local sub-geometry. We achieve such property with local contact frame referencing in training as well as with careful architectural design to preserve locality [19, 20, 15].

6 Related Works

Equivariant Robot Learning. Several recent works utilize the planar roto-translation equivariance, or the $SE(2)$ -equivariance to improve data-efficiency, generalizability, and robustness in robot learning with behavior cloning [12, 16, 48–52] and reinforcement learning [18, 53–55]. These approaches have also been shown to be effective for problems that are not strictly $SE(2)$ -symmetric [56, 57]. However, these methods suffer with highly spatial out-of-plane robotic manipulation tasks [19, 21]. To address this issue, incorporating the full spatial roto-translation equivariance, or the $SE(3)$ -equivariance has been explored [13, 14, 19, 15, 20, 17, 9, 10]. Equivariant modeling has also been shown to be effective for learning robot control [20, 58–60].

$SE(3)$ -Equivariant Graph Neural Networks. $SO(3)$ - and $SE(3)$ -equivariant graph neural networks (GNNs) [38, 39, 61, 62, 42, 63, 64] are widely used to model the 3-dimensional roto-translation symmetry in various domains including bioinformatics [65–67, 24, 23], chemistry [38, 39, 42, 68], computer vision [40, 41, 69–71], and robotics [13, 19, 17, 72]. In this paper, we use Equiformer [42] for the $SE(3)$ -equivariant GNN layers.

Diffusion Models. Diffusion models are rapidly replacing previous generative models in various fields including computer vision [44, 73–78], bioinformatics [23, 24, 79, 80], and robotics [1–11, 81, 82]. In particular, recent works studied diffusion-based generative modeling for non-Euclidean Riemannian manifolds [33, 34] such as Lie groups [27, 28, 7, 24, 23, 5]. In robotics, Urain et al. [7], Simeonov et al. [5] apply diffusion-based generative modeling directly on the end-effector pose space, which is the $SE(3)$ manifold. The application of diffusion guidance is also explored in robotics to modulate the denoising process so that actions with higher reward or lower cost are more likely to be sampled [1, 7, 8, 11]. $SE(3)$ -equivariant diffusion models on the product space of $SE(3)$ has been explored in bioinformatics [23, 24] but not yet in robotics.

7 Conclusion

In this paper, we demonstrate the required conditions as well as specific models and algorithms to incorporate the bi-equivariance in diffusion-based generative modeling on $SE(3)$ with point cloud observations of the scene and grasp. Our proposed method, Diffusion-EDFs, significantly enhance the slow training time and instability of EDFs without losing the end-to-end trainability. By experiment, we show that Diffusion-EDFs trained with only a few task demonstrations can be generalized to previously unseen object instances and poses, as well as the existence of previously unseen cluttered distracting objects. In practice, however, the observed point clouds are often noisy and with occlusions. Future research may explore methods that work directly from images to address this issue. Another limitation of Diffusion-EDFs is the inability of control-level or trajectory-level inference. The application of geometric control framework [83, 59] or guided diffusion with motion planning cost [1, 7] can be considered in subsequent works.

Acknowledgments and Disclosure of Funding

This work was supported by the National Research Foundation of Korea (NRF) grants funded by the Korea government (MSIT) (No.RS-2023-00221762 and No. 2021R1A2B5B01002620). This

work was also supported by the Korea Institute of Science and Technology (KIST) intramural grants (2E31570), and a Berkeley Fellowship.

References

- [1] Michael Janner, Yilun Du, Joshua B Tenenbaum, and Sergey Levine. Planning with diffusion for flexible behavior synthesis. *arXiv preprint arXiv:2205.09991*, 2022.
- [2] Kevin Black, Michael Janner, Yilun Du, Ilya Kostrikov, and Sergey Levine. Training diffusion models with reinforcement learning. *arXiv preprint arXiv:2305.13301*, 2023.
- [3] Tim Pearce, Tabish Rashid, Anssi Kanervisto, Dave Bignell, Mingfei Sun, Raluca Georgescu, Sergio Valcarcel Macua, Shan Zheng Tan, Ida Momennejad, Katja Hofmann, et al. Imitating human behaviour with diffusion models. *arXiv preprint arXiv:2301.10677*, 2023.
- [4] Cheng Chi, Siyuan Feng, Yilun Du, Zhenjia Xu, Eric Cousineau, Benjamin Burchfiel, and Shuran Song. Diffusion policy: Visuomotor policy learning via action diffusion. *arXiv preprint arXiv:2303.04137*, 2023.
- [5] Anthony Simeonov, Ankit Goyal, Lucas Manuelli, Lin Yen-Chen, Alina Sarmiento, Alberto Rodriguez, Pulkit Agrawal, and Dieter Fox. Shelving, stacking, hanging: Relational pose diffusion for multi-modal rearrangement. *arXiv preprint arXiv:2307.04751*, 2023.
- [6] Weiyu Liu, Tucker Hermans, Sonia Chernova, and Chris Paxton. Structdiffusion: Object-centric diffusion for semantic rearrangement of novel objects. *arXiv preprint arXiv:2211.04604*, 2022.
- [7] Julen Urain, Niklas Funk, Jan Peters, and Georgia Chalvatzaki. SE(3)-diffusionfields: Learning smooth cost functions for joint grasp and motion optimization through diffusion. *IEEE International Conference on Robotics and Automation (ICRA)*, 2023.
- [8] Anurag Ajay, Yilun Du, Abhi Gupta, Joshua Tenenbaum, Tommi Jaakkola, and Pulkit Agrawal. Is conditional generative modeling all you need for decision-making? *arXiv preprint arXiv:2211.15657*, 2022.
- [9] Johann Brehmer, Joey Bose, Pim De Haan, and Taco Cohen. Edgi: Equivariant diffusion for planning with embodied agents. *arXiv preprint arXiv:2303.12410*, 2023.
- [10] Johann Brehmer, Pim De Haan, Sönke Behrends, and Taco Cohen. Geometric algebra transformers. *arXiv preprint arXiv:2305.18415*, 2023.
- [11] Utkarsh A Mishra and Yongxin Chen. Reorientdiff: Diffusion model based reorientation for object manipulation. *arXiv preprint arXiv:2303.12700*, 2023.
- [12] Andy Zeng, Pete Florence, Jonathan Tompson, Stefan Welker, Jonathan Chien, Maria Attarian, Travis Armstrong, Ivan Krasin, Dan Duong, Vikas Sindhwani, and Johnny Lee. Transporter networks: Rearranging the visual world for robotic manipulation. *Conference on Robot Learning (CoRL)*, 2020.
- [13] Anthony Simeonov, Yilun Du, Andrea Tagliasacchi, Joshua B Tenenbaum, Alberto Rodriguez, Pulkit Agrawal, and Vincent Sitzmann. Neural descriptor fields: SE(3)-equivariant object representations for manipulation. In *2022 International Conference on Robotics and Automation (ICRA)*, pages 6394–6400. IEEE, 2022.
- [14] Anthony Simeonov, Yilun Du, Yen-Chen Lin, Alberto Rodriguez Garcia, Leslie Pack Kaelbling, Tomás Lozano-Pérez, and Pulkit Agrawal. SE(3)-equivariant relational rearrangement with neural descriptor fields. In *Conference on Robot Learning*, pages 835–846. PMLR, 2023.
- [15] Ethan Chun, Yilun Du, Anthony Simeonov, Tomas Lozano-Perez, and Leslie Kaelbling. Local neural descriptor fields: Locally conditioned object representations for manipulation. *arXiv preprint arXiv:2302.03573*, 2023.
- [16] Haojie Huang, Dian Wang, Robin Walters, and Robert Platt. Equivariant transporter network. *arXiv preprint arXiv:2202.09400*, 2022.
- [17] Haojie Huang, Dian Wang, Xupeng Zhu, Robin Walters, and Robert Platt. Edge grasp network: A graph-based SE(3)-invariant approach to grasp detection. In *2023 IEEE International Conference on Robotics and Automation (ICRA)*, pages 3882–3888. IEEE, 2023.
- [18] Dian Wang, Robin Walters, Xupeng Zhu, and Robert Platt. Equivariant q learning in spatial action spaces. In *Conference on Robot Learning*, pages 1713–1723. PMLR, 2022.

[19] Hyunwoo Ryu, Hong in Lee, Jeong-Hoon Lee, and Jongeun Choi. Equivariant descriptor fields: SE(3)-equivariant energy-based models for end-to-end visual robotic manipulation learning. In *The Eleventh International Conference on Learning Representations*, 2023. URL <https://openreview.net/forum?id=dnjZSPGmY50>.

[20] Jiwoo Kim, Hyunwoo Ryu, Jongeun Choi, Joohwan Seo, Nikhil Potu Surya Prakash, Ruolin Li, and Roberto Horowitz. Robotic manipulation learning with equivariant descriptor fields: Generative modeling, bi-equivariance, steerability, and locality. In *RSS 2023 Workshop on Symmetries in Robot Learning*, 2023.

[21] Yen-Chen Lin, Pete Florence, Andy Zeng, Jonathan T Barron, Yilun Du, Wei-Chiu Ma, Anthony Simeonov, Alberto Rodriguez Garcia, and Phillip Isola. Mira: Mental imagery for robotic affordances. In *Conference on Robot Learning*, pages 1916–1927. PMLR, 2023.

[22] Mario Geiger and Tess Smidt. e3nn: Euclidean neural networks, 2022. URL <https://arxiv.org/abs/2207.09453>.

[23] Jason Yim, Brian L Trippe, Valentin De Bortoli, Emile Mathieu, Arnaud Doucet, Regina Barzilay, and Tommi Jaakkola. SE(3) diffusion model with application to protein backbone generation. *arXiv preprint arXiv:2302.02277*, 2023.

[24] Gabriele Corso, Hannes Stärk, Bowen Jing, Regina Barzilay, and Tommi Jaakkola. Diffdock: Diffusion steps, twists, and turns for molecular docking. *International Conference on Learning Representations (ICLR)*, 2023.

[25] Dmitry I Nikolayev and Tatjana I Savoyolov. Normal distribution on the rotation group SO(3). *Textures and Microstructures*, 29, 1970.

[26] TM Ivanova TI Savoyolova. Normal distributions on SO(3). In *Programming And Mathematical Techniques In Physics-Proceedings Of The Conference On Programming And Mathematical Methods For Solving Physical Problems*, page 220. World Scientific, 1994.

[27] Adam Leach, Sebastian M Schmon, Matteo T Degiacomi, and Chris G Willcocks. Denoising diffusion probabilistic models on SO(3) for rotational alignment. In *ICLR 2022 Workshop on Geometrical and Topological Representation Learning*, 2022.

[28] Yesukhei Jagvaral, Francois Lanusse, and Rachel Mandelbaum. Diffusion generative models on SO(3). 2022.

[29] Roger Brockett. Notes on stochastic processes on manifolds. In *Systems and Control in the Twenty-first Century*, pages 75–100. Springer, 1997.

[30] Gregory S Chirikjian. *Stochastic models, information theory, and Lie groups, volume 2: Analytic methods and modern applications*, volume 2. Springer Science & Business Media, 2011.

[31] Yang Song and Stefano Ermon. Generative modeling by estimating gradients of the data distribution. *Advances in neural information processing systems*, 32, 2019.

[32] Frederic Koehler, Alexander Heckett, and Andrej Risteski. Statistical efficiency of score matching: The view from isoperimetry. *arXiv preprint arXiv:2210.00726*, 2022.

[33] Valentin De Bortoli, Emile Mathieu, Michael John Hutchinson, James Thornton, Yee Whye Teh, and Arnaud Doucet. Riemannian score-based generative modelling. In Alice H. Oh, Alekh Agarwal, Danielle Belgrave, and Kyunghyun Cho, editors, *Advances in Neural Information Processing Systems*, 2022. URL <https://openreview.net/forum?id=oDRQGo8I7P>.

[34] Chin-Wei Huang, Milad Aghajohari, Joey Bose, Prakash Panangaden, and Aaron C Courville. Riemannian diffusion models. *Advances in Neural Information Processing Systems*, 35:2750–2761, 2022.

[35] Richard M Murray, Zexiang Li, and S Shankar Sastry. *A mathematical introduction to robotic manipulation*. CRC press, 2017.

[36] Anthony Zee. *Group theory in a nutshell for physicists*, volume 17. Princeton University Press, 2016.

[37] Kevin M Lynch and Frank C Park. *Modern robotics*. Cambridge University Press, 2017.

[38] Nathaniel Thomas, Tess Smidt, Steven Kearnes, Lusann Yang, Li Li, Kai Kohlhoff, and Patrick Riley. Tensor field networks: Rotation-and translation-equivariant neural networks for 3d point clouds. *arXiv preprint arXiv:1802.08219*, 2018.

[39] Fabian Fuchs, Daniel Worrall, Volker Fischer, and Max Welling. SE(3)-transformers: 3d roto-translation equivariant attention networks. *Advances in neural information processing systems*, 33:1970–1981, 2020.

[40] Evangelos Chatzipantazis, Stefanos Pertigkiozoglou, Edgar Dobriban, and Kostas Daniilidis. SE(3)-equivariant attention networks for shape reconstruction in function space. *arXiv preprint arXiv:2204.02394*, 2022.

[41] Congyue Deng, Jiahui Lei, Bokui Shen, Kostas Daniilidis, and Leonidas Guibas. Banana: Banach fixed-point network for pointcloud segmentation with inter-part equivariance. *arXiv preprint arXiv:2305.16314*, 2023.

[42] Yi-Lun Liao and Tess Smidt. Equiformer: Equivariant graph attention transformer for 3d atomistic graphs. *arXiv preprint arXiv:2206.11990*, 2022.

[43] Charles Ruizhongtai Qi, Li Yi, Hao Su, and Leonidas J Guibas. Pointnet++: Deep hierarchical feature learning on point sets in a metric space. *Advances in neural information processing systems*, 30, 2017.

[44] Jonathan Ho, Ajay Jain, and Pieter Abbeel. Denoising diffusion probabilistic models. *Advances in neural information processing systems*, 33:6840–6851, 2020.

[45] Ondrej Biza, Skye Thompson, Kishore Reddy Pagidi, Abhinav Kumar, Elise van der Pol, Robin Walters, Thomas Kipf, Jan-Willem van de Meent, Lawson LS Wong, and Robert Platt. One-shot imitation learning via interaction warping. *arXiv preprint arXiv:2306.12392*, 2023.

[46] Fanbo Xiang, Yuzhe Qin, Kaichun Mo, Yikuan Xia, Hao Zhu, Fangchen Liu, Minghua Liu, Hanxiao Jiang, Yifu Yuan, He Wang, Li Yi, Angel X. Chang, Leonidas J. Guibas, and Hao Su. SAPIEN: A simulated part-based interactive environment. In *The IEEE Conference on Computer Vision and Pattern Recognition (CVPR)*, June 2020.

[47] Angel X Chang, Thomas Funkhouser, Leonidas Guibas, Pat Hanrahan, Qixing Huang, Zimo Li, Silvio Savarese, Manolis Savva, Shuran Song, Hao Su, et al. Shapenet: An information-rich 3d model repository. *arXiv preprint arXiv:1512.03012*, 2015.

[48] Daniel Seita, Pete Florence, Jonathan Tompson, Erwin Coumans, Vikas Sindhwani, Ken Goldberg, and Andy Zeng. Learning to rearrange deformable cables, fabrics, and bags with goal-conditioned transporter networks. In *2021 IEEE International Conference on Robotics and Automation (ICRA)*, pages 4568–4575. IEEE, 2021.

[49] Hongtao Wu, Jikai Ye, Xin Meng, Chris Paxton, and Gregory S Chirikjian. Transporters with visual foresight for solving unseen rearrangement tasks. In *2022 IEEE/RSJ International Conference on Intelligent Robots and Systems (IROS)*, pages 10756–10763. IEEE, 2022.

[50] Yadong Teng, Huimin Lu, Yujie Li, Tohru Kamiya, Yoshihisa Nakatoh, Seiichi Serikawa, and Pengxiang Gao. Multidimensional deformable object manipulation based on dn-transporter networks. *IEEE Transactions on Intelligent Transportation Systems*, 24(4):4532–4540, 2022.

[51] Michael H Lim, Andy Zeng, Brian Ichter, Maryam Bandari, Erwin Coumans, Claire Tomlin, Stefan Schaal, and Aleksandra Faust. Multi-task learning with sequence-conditioned transporter networks. In *2022 International Conference on Robotics and Automation (ICRA)*, pages 2489–2496. IEEE, 2022.

[52] Mingxi Jia, Dian Wang, Guanang Su, David Klee, Xupeng Zhu, Robin Walters, and Robert Platt. Seil: Simulation-augmented equivariant imitation learning. In *2023 IEEE International Conference on Robotics and Automation (ICRA)*, pages 1845–1851. IEEE, 2023.

[53] Dian Wang, Robin Walters, and Robert Platt. SO(2)-equivariant reinforcement learning. *arXiv preprint arXiv:2203.04439*, 2022.

[54] Xupeng Zhu, Dian Wang, Ondrej Biza, Guanang Su, Robin Walters, and Robert Platt. Sample efficient grasp learning using equivariant models. *arXiv preprint arXiv:2202.09468*, 2022.

[55] Dian Wang, Mingxi Jia, Xupeng Zhu, Robin Walters, and Robert Platt. On-robot learning with equivariant models. *arXiv preprint arXiv:2203.04923*, 2022.

[56] Dian Wang, Jung Yeon Park, Neel Sortur, Lawson LS Wong, Robin Walters, and Robert Platt. The surprising effectiveness of equivariant models in domains with latent symmetry. *arXiv preprint arXiv:2211.09231*, 2022.

[57] Dian Wang, Xupeng Zhu, Jung Yeon Park, Robert Platt, and Robin Walters. A general theory of correct, incorrect, and extrinsic equivariance. *arXiv preprint arXiv:2303.04745*, 2023.

[58] Linfeng Zhao, Jung Yeon Park, Xupeng Zhu, Robin Walters, and Lawson LS Wong. SE(3) frame equivariance in dynamics modeling and reinforcement learning. In *ICLR 2023 Workshop on Physics for Machine Learning*, 2023.

[59] Joohwan Seo, Nikhil Potu Surya Prakash, Xiang Zhang, Changhao Wang, Jongeun Choi, Masayoshi Tomizuka, and Roberto Horowitz. Robot manipulation task learning by leveraging SE(3) group invariance and equivariance. *arXiv preprint arXiv:2308.14984*, 2023.

[60] Colin Kohler, Anuj Shrivatsav Srikanth, Eshan Arora, and Robert Platt. Symmetric models for visual force policy learning. *arXiv preprint arXiv:2308.14670*, 2023.

[61] Victor Garcia Satorras, Emiel Hoogeboom, and Max Welling. E(n) equivariant graph neural networks. In *International conference on machine learning*, pages 9323–9332. PMLR, 2021.

[62] Congyue Deng, Or Litany, Yueqi Duan, Adrien Poulenard, Andrea Tagliasacchi, and Leonidas J Guibas. Vector neurons: A general framework for SO(3)-equivariant networks. In *Proceedings of the IEEE/CVF International Conference on Computer Vision*, pages 12200–12209, 2021.

[63] Weitao Du, He Zhang, Yuanqi Du, Qi Meng, Wei Chen, Nanning Zheng, Bin Shao, and Tie-Yan Liu. SE(3) equivariant graph neural networks with complete local frames. In *International Conference on Machine Learning*, pages 5583–5608. PMLR, 2022.

[64] Yi-Lun Liao, Brandon Wood, Abhishek Das, and Tess Smidt. Equiformerv2: Improved equivariant transformer for scaling to higher-degree representations. *arXiv preprint arXiv:2306.12059*, 2023.

[65] Patrick Cramer. Alphafold2 and the future of structural biology. *Nature structural & molecular biology*, 28(9):704–705, 2021.

[66] Jae Hyeon Lee, Payman Yadollahpour, Andrew Watkins, Nathan C Frey, Andrew Leaver-Fay, Stephen Ra, Kyunghyun Cho, Vladimir Gligorijević, Aviv Regev, and Richard Bonneau. Equifold: Protein structure prediction with a novel coarse-grained structure representation. *bioRxiv*, pages 2022–10, 2022.

[67] Octavian-Eugen Ganea, Xinyuan Huang, Charlotte Bunne, Yatao Bian, Regina Barzilay, Tommi Jaakkola, and Andreas Krause. Independent SE(3)-equivariant models for end-to-end rigid protein docking. *arXiv preprint arXiv:2111.07786*, 2021.

[68] Simon Batzner, Albert Musaelian, Lixin Sun, Mario Geiger, Jonathan P Mailoa, Mordechai Kornbluth, Nicola Molinari, Tess E Smidt, and Boris Kozinsky. E(3)-equivariant graph neural networks for data-efficient and accurate interatomic potentials. *Nature communications*, 13(1):2453, 2022.

[69] Chien Erh Lin, Jingwei Song, Ray Zhang, Minghan Zhu, and Maani Ghaffari. SE(3)-equivariant point cloud-based place recognition. In *Conference on Robot Learning*, pages 1520–1530. PMLR, 2023.

[70] Minghan Zhu, Maani Ghaffari, William A Clark, and Huei Peng. E2pn: Efficient SE(3)-equivariant point network. In *Proceedings of the IEEE/CVF Conference on Computer Vision and Pattern Recognition*, pages 1223–1232, 2023.

[71] Jiahui Lei, Congyue Deng, Karl Schmeckpeper, Leonidas Guibas, and Kostas Daniilidis. Efem: Equivariant neural field expectation maximization for 3d object segmentation without scene supervision. In *Proceedings of the IEEE/CVF Conference on Computer Vision and Pattern Recognition*, pages 4902–4912, 2023.

[72] Jiahui Fu, Yilun Du, Kurran Singh, Joshua B Tenenbaum, and John J Leonard. Neuse: Neural SE(3)-equivariant embedding for consistent spatial understanding with objects. *arXiv preprint arXiv:2303.07308*, 2023.

[73] Jiaming Song, Chenlin Meng, and Stefano Ermon. Denoising diffusion implicit models. *arXiv preprint arXiv:2010.02502*, 2020.

[74] Yang Song, Jascha Sohl-Dickstein, Diederik P Kingma, Abhishek Kumar, Stefano Ermon, and Ben Poole. Score-based generative modeling through stochastic differential equations. *arXiv preprint arXiv:2011.13456*, 2020.

[75] Prafulla Dhariwal and Alexander Nichol. Diffusion models beat gans on image synthesis. *Advances in neural information processing systems*, 34:8780–8794, 2021.

[76] Aditya Ramesh, Prafulla Dhariwal, Alex Nichol, Casey Chu, and Mark Chen. Hierarchical text-conditional image generation with clip latents. *arXiv preprint arXiv:2204.06125*, 1(2):3, 2022.

[77] Alex Nichol, Prafulla Dhariwal, Aditya Ramesh, Pranav Shyam, Pamela Mishkin, Bob McGrew, Ilya Sutskever, and Mark Chen. Glide: Towards photorealistic image generation and editing with text-guided diffusion models. *arXiv preprint arXiv:2112.10741*, 2021.

[78] Robin Rombach, Andreas Blattmann, Dominik Lorenz, Patrick Esser, and Björn Ommer. High-resolution image synthesis with latent diffusion models. In *Proceedings of the IEEE/CVF conference on computer vision and pattern recognition*, pages 10684–10695, 2022.

[79] Joseph L Watson, David Juergens, Nathaniel R Bennett, Brian L Trippe, Jason Yim, Helen E Eisenach, Woody Ahern, Andrew J Borst, Robert J Ragotte, Lukas F Milles, et al. Broadly applicable and accurate protein design by integrating structure prediction networks and diffusion generative models. *BioRxiv*, pages 2022–12, 2022.

[80] Yilun Du, Conor Durkan, Robin Strudel, Joshua B Tenenbaum, Sander Dieleman, Rob Fergus, Jascha Sohl-Dickstein, Arnaud Doucet, and Will Sussman Grathwohl. Reduce, reuse, recycle: Compositional generation with energy-based diffusion models and mcmc. In *International Conference on Machine Learning*, pages 8489–8510. PMLR, 2023.

[81] Hongyi Chen, Yilun Du, Yiye Chen, Joshua Tenenbaum, and Patricio A Vela. Planning with sequence models through iterative energy minimization. *arXiv preprint arXiv:2303.16189*, 2023.

[82] Yilun Dai, Mengjiao Yang, Bo Dai, Hanjun Dai, Ofir Nachum, Josh Tenenbaum, Dale Schuurmans, and Pieter Abbeel. Learning universal policies via text-guided video generation. *arXiv preprint arXiv:2302.00111*, 2023.

[83] Joohwan Seo, Nikhil Potu Surya Prakash, Alexander Rose, and Roberto Horowitz. Geometric impedance control on SE(3) for robotic manipulators. *arXiv preprint arXiv:2211.07945*, 2022.

[84] Gregory S Chirikjian. Partial bi-invariance of SE(3) metrics. *Journal of Computing and Information Science in Engineering*, 15(1), 2015.

[85] Gregory S Chirikjian. *Engineering applications of noncommutative harmonic analysis: with emphasis on rotation and motion groups*. CRC press, 2000.

[86] Alexander B Kyatkin and Gregory S Chirikjian. Regularized solutions of a nonlinear convolution equation on the euclidean group. *Acta Applicandae Mathematica*, 53:89–123, 1998.

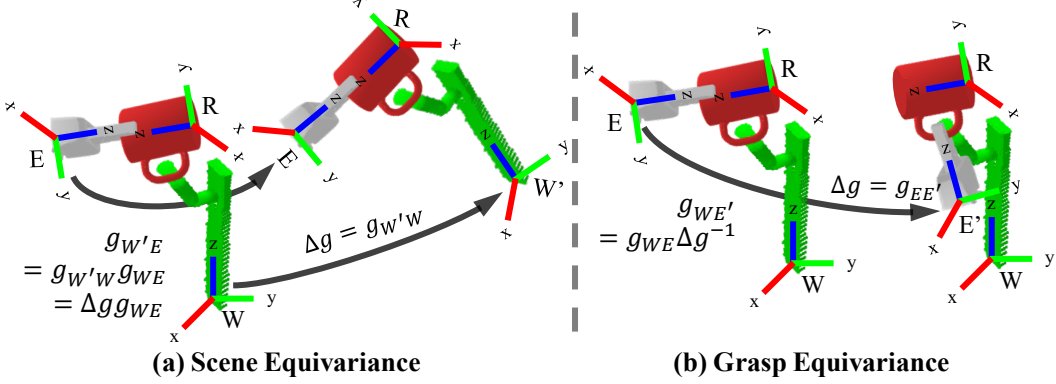


Figure 4: **Scene Equivariance and Grasp Equivariance.** (a) The end-effector pose must follow the transformation of the placement target within the scene. This *scene equivariance* can be achieved by multiplying the transformation Δg on the left side of the end-effector pose. Therefore, we also refer to this property as the *left equivariance*. (b) The end-effector pose must move contravariantly to the transformation of the grasped object to compensate for the changes. This *grasp equivariance* involves the inverse transformation Δg^{-1} coming to the right side of the end-effector pose. Therefore, we also refer to this property as the *right equivariance*.

A Bi-equivariance

For robust pick-and-place manipulation, the trained policy needs to be generalizable to previously unseen configurations of the target objects to pick/place. This can be achieved by inferring end-effector poses that keep the relative pose between the grasped object and the placement target. Note that in our formulation, picking is essentially a special case of placing tasks, in which the gripper is *placed* at appropriate grasp points of the target object to pick with an appropriate orientation.

Consider the scenario in which the policy is trained with a demonstration $(g_{WE}, O^{(s)}, O^{(b)})$ in which g_{WE} is the end-effector pose, and $O^{(s)}$ and $O^{(b)}$ are respectively the point cloud observations of the scene and grasp. We denote the world frame using subscript W and the end-effector frame using subscript E . Note that $O^{(s)}$ is observed in frame W and $O^{(b)}$ in frame E . Now, let the placement target be moved by $\Delta g = g_{W'W}$, inducing the transformation of the observation $O^{(s)} \rightarrow \Delta g O^{(s)}$. This is equivalent to changing the world reference frame from W to W' with respect to the observation. Therefore, the end-effector pose should also be transformed equivariantly as $g_{WE} \rightarrow g_{W'E} = \Delta g g_{WE}$ (see Figure 4-(a)). This *scene equivariance* is also referred to as *left equivariance* [19, 20], as the transformation Δg comes to the left side of g_{WE} .

On the other hand, consider the transformation of the grasped object $\Delta g = g_{E'E}$, which induces the transformation of the observation $O^{(b)} \rightarrow \Delta g O^{(b)}$. This is equivalent to changing the end-effector reference frame from E to E' with respect to the observation. In the world frame, this corresponds to the transformation of the end-effector pose by $g_{WE} \rightarrow g_{WE'} = g_{WE} \Delta g^{-1}$ (see Figure 4-(b)). This *grasp equivariance* is also referred to as *right equivariance* [19, 20], as the transformation Δg^{-1} comes to the right side of g_{WE} . Combining these left and right equivariance conditions, we obtain the bi-equivariance condition, which can be formally expressed in a probabilistic form as Equation (8).

B Analytic Form of the Target Score in Equation (20)

In this section, we provide the analytic form of the target score function in Equation (20)

$$\nabla \log \mathcal{B}_t(g_{ref}^{-1} g_0^{-1} g g_{ref}) \quad (35)$$

By definition, the i -th component of the target score function is calculated as follows:

$$\begin{aligned}
\mathcal{L}_i \log \mathcal{B}_t(g_{ref}^{-1} g_0^{-1} g g_{ref}) &= \frac{d}{d\epsilon} \bigg|_{\epsilon=0} \log \mathcal{B}_t \left(g_{ref}^{-1} g_0^{-1} g \exp[\epsilon \hat{\mathbf{e}}_i] g_{ref} \right) \\
&= \frac{d}{d\epsilon} \bigg|_{\epsilon=0} \log \mathcal{B}_t \left(g_{ref}^{-1} g_0^{-1} g g_{ref} \exp[\epsilon A d_{g_{ref}^{-1}} \hat{\mathbf{e}}_i] \right) \\
&= \left[\mathcal{L}_{Ad_{g_{ref}^{-1}} \hat{\mathbf{e}}_i} \log \mathcal{B}_t \right] \left(g_{ref}^{-1} g_0^{-1} g g_{ref} \right) \\
&= \left[\sum_{j=1}^6 \left[Ad_{g_{ref}^{-1}} \right]_{ji} \mathcal{L}_j \log \mathcal{B}_t \right] \left(g_{ref}^{-1} g_0^{-1} g g_{ref} \right) \\
&= \sum_{j=1}^6 \left[Ad_{g_{ref}^{-1}} \right]_{ji} \left[\mathcal{L}_j \log \mathcal{B}_t \right] \left(g_{ref}^{-1} g_0^{-1} g g_{ref} \right) \\
\Rightarrow \nabla \log \mathcal{B}_t(g_{ref}^{-1} g_0^{-1} g g_{ref}) &= \left[Ad_{g_{ref}} \right]^{-T} \left[\nabla \log \mathcal{B}_t \right] \left(g_{ref}^{-1} g_0^{-1} g g_{ref} \right) \quad (36)
\end{aligned}$$

Therefore, all we need is the score of the Brownian diffusion kernel $\nabla \log \mathcal{B}_t(g)$ which can be decomposed into its translation and rotation parts using Equation (4)

$$\nabla \log \mathcal{B}_t(g) = \nabla \log \mathcal{N}(\mathbf{p}; \boldsymbol{\mu} = \mathbf{0}, \Sigma = tI) + \nabla \log \mathcal{IG}_{SO(3)}(R; \epsilon = t/2)$$

where $\nabla \log \mathcal{N}(\mathbf{p}; \boldsymbol{\mu} = \mathbf{0}, \Sigma = tI) = -\mathbf{p}/t$ can be easily computed. A common practice for the calculation of the rotational part $\nabla \log \mathcal{IG}_{SO(3)}(R; \epsilon = t/2)$ is to use automatic differentiation packages [27, 19, 28, 7, 24, 23]. However, the explicit form can be easily calculated without automatic differentiation packages.

$$\mathcal{L}_i \log \mathcal{IG}_{SO(3)}(R; \epsilon) = \frac{\mathcal{L}_i \mathcal{IG}_{SO(3)}(R; \epsilon)}{\mathcal{IG}_{SO(3)}(R; \epsilon)} \quad (37)$$

$$\begin{aligned}
&\mathcal{L}_i \mathcal{IG}_{SO(3)}(R; \epsilon) \\
&= \sum_{l=0}^{\infty} (2l+1) \exp[-l(l+1)\epsilon] \left[\frac{(l+1) \sin(l\theta) - l \sin((l+1)\theta)}{\cos(\theta) - 1} \right] \left[\frac{-\text{tr}[R[\hat{\mathbf{e}}_i]^\wedge]}{2 \sin \theta} \right] \quad (38)
\end{aligned}$$

We denote the skew-symmetric matrix of the i -th $\mathfrak{so}(3)$ basis $\hat{\mathbf{e}}_i$ as $[\hat{\mathbf{e}}_i]^\wedge$, whose matrix element is $[\hat{\mathbf{e}}_i]_{jk}^\wedge = -\epsilon_{ijk}$ where ϵ_{ijk} is the Levi-Civita symbol.

The derivation is as follows. First, we rewrite Equation (5) with the *character* $\mathcal{X}(R)$ of $SO(3)$ [36].

$$\begin{aligned}
\mathcal{IG}_{SO(3)}(R; \epsilon) &= \sum_{l=0}^{\infty} (2l+1) \exp[-l(l+1)\epsilon] \mathcal{X}_l(R) \\
\mathcal{X}_l(R) &= \text{tr}[D_l(R)] = \sin\left((2l+1)\frac{\theta}{2}\right) / \sin(\frac{\theta}{2})
\end{aligned}$$

$\theta \in (0, \pi)$ is the rotation angle of R . Now we calculate the Lie derivative of $\mathcal{IG}_{SO(3)}$ as follows:

$$\begin{aligned}
\mathcal{L}_i \mathcal{IG}_{SO(3)}(R; \epsilon) &= \sum_{l=0}^{\infty} (2l+1) \exp[-l(l+1)\epsilon] \mathcal{L}_i \mathcal{X}_l(R) \\
\mathcal{L}_i \mathcal{X}_l(R) &= \left[\frac{(l+1) \sin(l\theta) - l \sin((l+1)\theta)}{\cos(\theta) - 1} \right] \mathcal{L}_i \theta \\
\mathcal{L}_i \theta &= \left[\frac{-1}{\sin \theta} \right] \mathcal{L}_i [\cos \theta]
\end{aligned}$$

The last line can be easily calculated using $\cos \theta = \frac{1}{2} (\text{tr}[R] - 1)$ and $\mathcal{L}_V \text{tr}[R] = \text{tr}[R[V]^\wedge]$.

$$\mathcal{L}_i [\cos \theta] = \frac{1}{2} (\text{tr}[R[\hat{\mathbf{e}}_i]^\wedge])$$

Combining these results, one can derive Equation (38). In practice, the infinite sum in Equation (38) is approximated with $\sum_{l=0}^{l_{max}}$ where $l_{max} = 1000 \sim 10000$, which can be computed within a millisecond when appropriately parallelized. Although we have derived Equation (38) for $\theta = (0, \pi)$, the result can be asymptotically extended to $\theta = 0$ and π as $\mathcal{IG}_{SO(3)}$ is infinitely differentiable [25].

C Proofs and Derivations

C.1 Proof of Proposition 1

Proof of the left invariance of the score function.

$$\begin{aligned}
\mathcal{L}_i \log P(\Delta g | \Delta g \cdot O^{(s)}, O^{(b)}) &= \frac{d}{d\epsilon} \bigg|_{\epsilon=0} \log P(\Delta g g \exp [\epsilon \hat{e}_i] | \Delta g \cdot O^{(s)}, O^{(b)}) \\
&= \frac{d}{d\epsilon} \bigg|_{\epsilon=0} \log P(g \exp [\epsilon \hat{e}_i] | O^{(s)}, O^{(b)}) \\
&= \mathcal{L}_i \log P(g | O^{(s)}, O^{(b)})
\end{aligned}$$

where we used $P(\Delta g g | \Delta g \cdot O^{(s)}, O^{(b)}) = P(g | O^{(s)}, O^{(b)})$ in the second line. \square

Proof of the right equivariance of the score function.

$$\begin{aligned}
\mathcal{L}_i \log P(g \Delta g^{-1} | O^{(s)}, \Delta g \cdot O^{(b)}) &= \frac{d}{d\epsilon} \bigg|_{\epsilon=0} \log P(g \Delta g^{-1} \exp [\epsilon \hat{e}_i] | O^{(s)}, \Delta g \cdot O^{(b)}) \\
&= \frac{d}{d\epsilon} \bigg|_{\epsilon=0} \log P(g \Delta g^{-1} \exp [\epsilon \hat{e}_i] \Delta g | O^{(s)}, O^{(b)}) \\
&= \frac{d}{d\epsilon} \bigg|_{\epsilon=0} \log P(g \exp [\epsilon Ad_{\Delta g^{-1}} \hat{e}_i] | O^{(s)}, O^{(b)}) \\
&= \mathcal{L}_{Ad_{\Delta g^{-1}} \hat{e}_i} \log P(g | O^{(s)}, O^{(b)}) \\
&= \mathcal{L}_{\sum_j [Ad_{\Delta g^{-1}}]_{ji} \hat{e}_j} \log P(g | O^{(s)}, O^{(b)}) \\
&= \sum_{j=1}^6 [Ad_{\Delta g^{-1}}]_{ji} \mathcal{L}_j \log P(g | O^{(s)}, O^{(b)}) \\
&\quad (\because \text{Linearity of Lie-derivatives [30]} \quad \mathcal{L}_{\sum_i v_i \hat{e}_i} = \sum_i v_i \mathcal{L}_i) \\
\Rightarrow \nabla \log P(g \Delta g^{-1} | O^{(s)}, \Delta g \cdot O^{(b)}) &= [Ad_{\Delta g^{-1}}]^T \nabla \log P(g | O^{(s)}, O^{(b)}) \\
&= [Ad_{\Delta g}]^{-T} \nabla \log P(g | O^{(s)}, O^{(b)})
\end{aligned}$$

where we denote the (j, i) -th matrix element of $Ad_{\Delta g^{-1}}$ with $[Ad_{\Delta g^{-1}}]_{ji}$. We used $P(g \Delta g^{-1} | O^{(s)}, \Delta g \cdot O^{(b)}) = P(g | O^{(s)}, O^{(b)})$ in the second line. \square

C.2 Proof of Proposition 2

It is straightforward to prove the bi-equivariance of the diffused marginal using the bi-invariance of the integral measure (Haar measure) dg

$$\int_{g \in SE(3)} d(\Delta g g) = \int_{g \in SE(3)} dg = \int_{g \in SE(3)} d(g \Delta g) \quad \forall \Delta g \in SE(3) \quad (39)$$

where $dg = dR d\mathbf{p} = \frac{1}{8\pi^2} (\sin \beta) d\alpha d\beta d\gamma dx dy dz$ in the rotation-translation coordinate with the Euler angles α, β, γ and the frame origin x, y, z . See Chirikjian [84, 30, 85], Murray et al. [35] and Appendix A of Ryu et al. [19] for more details on the bi-invariant integral measure of $SE(3)$.

We first prove that the marginal is bi-equivariant if the kernel is bi-equivariant.

Proof of left equivariance.

$$\begin{aligned}
P_t(g|O^{(s)}, O^{(b)}) &= \int_{g_0 \in SE(3)} dg_0 P_{t|0}(g|g_0, O^{(s)}, O^{(b)}) P_0(g_0|O^{(s)}, O^{(b)}) \\
&= \int_{g_0 \in SE(3)} dg_0 P_{t|0}(g|g_0, O^{(s)}, O^{(b)}) P_0(\Delta g g_0|\Delta g \cdot O^{(s)}, O^{(b)}) \\
&\quad (\because \text{Equation (8)}) \\
&= \int_{g_0 \in SE(3)} dg_0 P_{t|0}(\Delta g g|\Delta g g_0, \Delta g \cdot O^{(s)}, O^{(b)}) P_0(\Delta g g_0|\Delta g \cdot O^{(s)}, O^{(b)}) \\
&\quad (\because \text{Equation (14)}) \\
&= \int_{g_0 \in SE(3)} dg_0 P_{t|0}(\Delta g g|g_0, \Delta g \cdot O^{(s)}, O^{(b)}) P_0(g_0|\Delta g \cdot O^{(s)}, O^{(b)}) \\
&\quad (\because \text{Equation (39), } \Delta g g_0 \rightarrow g_0) \\
&= P_t(\Delta g g|\Delta g \cdot O^{(s)}, O^{(b)})
\end{aligned}$$

□

Proof of right equivariance.

$$\begin{aligned}
P_t(g|O^{(s)}, O^{(b)}) &= \int_{g_0 \in SE(3)} dg_0 P_{t|0}(g|g_0, O^{(s)}, O^{(b)}) P_0(g_0|O^{(s)}, O^{(b)}) \\
&= \int_{g_0 \in SE(3)} dg_0 P_{t|0}(g|g_0, O^{(s)}, O^{(b)}) P_0(g_0 \Delta g^{-1}|O^{(s)}, \Delta g \cdot O^{(b)}) \\
&\quad (\because \text{Equation (8)}) \\
&= \int_{g_0 \in SE(3)} dg_0 P_{t|0}(g \Delta g^{-1}|g_0 \Delta g^{-1}, O^{(s)}, \Delta g \cdot O^{(b)}) P_0(g_0 \Delta g^{-1}|O^{(s)}, \Delta g \cdot O^{(b)}) \\
&\quad (\because \text{Equation (15)}) \\
&= \int_{g_0 \in SE(3)} dg_0 P_{t|0}(g \Delta g^{-1}|g_0, O^{(s)}, \Delta g \cdot O^{(b)}) P_0(g_0|O^{(s)}, \Delta g \cdot O^{(b)}) \\
&\quad (\because \text{Equation (39), } g_0 \Delta g^{-1} \rightarrow g_0) \\
&= P_t(g \Delta g^{-1}|O^{(s)}, \Delta g \cdot O^{(b)})
\end{aligned}$$

□

Similarly, it can be proven that the kernel must be bi-equivariant (up to measure zero) to guarantee the bi-equivariance of the diffused marginal for any arbitrary initial distribution $dP_0 = P_0 dg_0$.

Proof.

$$\begin{aligned}
P_t(g|O^{(s)}, O^{(b)}) &= \int_{g_0 \in SE(3)} dg_0 P_{t|0}(g|g_0, O^{(s)}, O^{(b)}) P_0(g_0|O^{(s)}, O^{(b)}) \\
P_t(\Delta g g|\Delta g \cdot O^{(s)}, O^{(b)}) &= \int_{g_0 \in SE(3)} dg_0 P_{t|0}(\Delta g g|g_0, \Delta g \cdot O^{(s)}, O^{(b)}) P_0(g_0|\Delta g \cdot O^{(s)}, O^{(b)}) \\
&= \int_{g_0 \in SE(3)} dg_0 P_{t|0}(\Delta g g|g_0, \Delta g \cdot O^{(s)}, O^{(b)}) P_0(\Delta g^{-1} g_0|O^{(s)}, O^{(b)}) \\
&\quad (\because \text{Equation (8)}) \\
&= \int_{g_0 \in SE(3)} dg_0 P_{t|0}(\Delta g g|\Delta g g_0, \Delta g \cdot O^{(s)}, O^{(b)}) P_0(g_0|O^{(s)}, O^{(b)}) \\
&\quad (\because \text{Equation (39), } g_0 \rightarrow \Delta g g_0)
\end{aligned}$$

$$\begin{aligned}
P_t(g \Delta g^{-1} | O^{(s)}, \Delta g \cdot O^{(b)}) &= \int_{g_0 \in SE(3)} dg_0 P_{t|0}(g \Delta g^{-1} | g_0, O^{(s)}, \Delta g \cdot O^{(b)}) P_0(g_0 | O^{(s)}, \Delta g \cdot O^{(b)}) \\
&= \int_{g_0 \in SE(3)} dg_0 P_{t|0}(g \Delta g^{-1} | g_0, O^{(s)}, \Delta g \cdot O^{(b)}) P_0(g_0 \Delta g | O^{(s)}, O^{(b)}) \\
&\quad (\because \text{Equation (8)}) \\
&= \int_{g_0 \in SE(3)} dg_0 P_{t|0}(g \Delta g^{-1} | g_0 \Delta g^{-1}, O^{(s)}, \Delta g \cdot O^{(b)}) P_0(g_0 | O^{(s)}, O^{(b)}) \\
&\quad (\because \text{Equation (39), } g_0 \rightarrow g_0 \Delta g^{-1})
\end{aligned}$$

$$\begin{aligned}
\Rightarrow \int dg_0 P_0(g_0 | O^{(s)}, O^{(b)}) \times \left[P_{t|0}(g | g_0, O^{(s)}, O^{(b)}) - P_{t|0}(\Delta g g | \Delta g g_0, \Delta g \cdot O^{(s)}, O^{(b)}) \right] &= 0 \\
\int dg_0 P_0(g_0 | O^{(s)}, O^{(b)}) \times \left[P_{t|0}(g | g_0, O^{(s)}, O^{(b)}) - P_{t|0}(g \Delta g^{-1} | g_0 \Delta g^{-1}, O^{(s)}, \Delta g \cdot O^{(b)}) \right] &= 0
\end{aligned}$$

Therefore, for this equation to hold for any arbitrary bi-equivariant initial distribution $dP_0 = P_0 dg_0$, the diffusion kernel must be bi-equivariant $\forall g, \Delta g \in SE(3)$

$$\begin{aligned}
P_{t|0}(g | g_0, O^{(s)}, O^{(b)}) - P_{t|0}(\Delta g g | \Delta g g_0, \Delta g \cdot O^{(s)}, O^{(b)}) &= 0 \\
P_{t|0}(g | g_0, O^{(s)}, O^{(b)}) - P_{t|0}(g \Delta g^{-1} | g_0 \Delta g^{-1}, O^{(s)}, \Delta g \cdot O^{(b)}) &= 0 \\
\Rightarrow P_{t|0}(g | g_0, O^{(s)}, O^{(b)}) &= P_{t|0}(\Delta g g | \Delta g g_0, \Delta g \cdot O^{(s)}, O^{(b)}) \\
&= P_{t|0}(g \Delta g^{-1} | g_0 \Delta g^{-1}, O^{(s)}, \Delta g \cdot O^{(b)})
\end{aligned}$$

□

C.3 Non-existence of Bi-Invariant Diffusion Kernels on SE(3)

Due to the left invariance of the kernel, it must depend solely on the group difference $g_0^{-1} g$

$$P_{t|0}(\Delta g g | \Delta g g_0) = P_{t|0}(g | g_0) \quad \forall \Delta g, g \quad \Rightarrow \quad P_{t|0}(g | g_0) = P_{t|0}(g_0^{-1} g | I) \quad \forall g$$

Therefore, we can simply denote any left-invariant kernel as $K_t(g) = P_{t|0}(g | I)$. The right invariance requires this kernel to satisfy $K_t(\Delta g g \Delta g^{-1}) = K_t(g)$, meaning that it is a *class function*, which does not exist for $L^2(SE(3))$ [86, 85].

C.4 Proof of Proposition 3

Proof. The right equivariance can be proved as follows.

$$\begin{aligned}
P_{t|0}(g | g_0, O^{(s)}, O^{(b)}) &= \int dg_{ref} P_{ref}(g_{ref} | g_0^{-1} \cdot O^{(s)}, O^{(b)}) K_t(g_{ref}^{-1} g_0^{-1} g g_{ref}) \\
&= \int dg_{ref} P_{ref}(\Delta g g_{ref} | (\Delta g g_0^{-1}) \cdot O^{(s)}, \Delta g \cdot O^{(b)}) K_t(g_{ref}^{-1} g_0^{-1} g g_{ref}) \\
&\quad (\because \text{Equation (17)}) \\
&= \int dg_{ref} P_{ref}(g_{ref} | (\Delta g g_0^{-1}) \cdot O^{(s)}, \Delta g \cdot O^{(b)}) K_t(g_{ref}^{-1} (g_0 \Delta g^{-1})^{-1} (g \Delta g^{-1}) g_{ref}) \\
&\quad (\because \text{invariance of integral } \int dg_{ref} \text{ under } g_{ref} \rightarrow \Delta g^{-1} g_{ref}) \\
&= P_{t|0}(g \Delta g^{-1} | g_0 \Delta g^{-1}, O^{(s)}, \Delta g \cdot O^{(b)})
\end{aligned}$$

The left equivariance proof is straightforward using the following equations:

$$\begin{aligned}
g_0^{-1} g &= (\Delta g g_0)^{-1} (\Delta g g) \\
g_0^{-1} \cdot O^{(s)} &= (\Delta g g_0)^{-1} \cdot (\Delta g \cdot O^{(s)})
\end{aligned}$$

□

C.5 Proof of Proposition 4

Note that the Brownian diffusion kernel $\mathcal{B}_t(g)$ is right-invariant to rotation, that is,

$$\begin{aligned} \mathcal{B}_t((g_0 \Delta R)^{-1} (g \Delta R)) &= \mathcal{B}_t(g_0^{-1} g) \\ \Rightarrow \mathcal{B}_t(\Delta R^{-1} g \Delta R) &= \mathcal{B}_t(g) \quad \forall \Delta R \in SO(3) \end{aligned} \quad (40)$$

where we abuse the notation to denote the action of a pure rotation ΔR on $g = (\mathbf{p}, R)$ as $\Delta R g = (\Delta R \mathbf{p}, \Delta R R)$ and $g \Delta R = (\mathbf{p}, R \Delta R)$. Equation (40) holds because the Gaussian distribution in Equation (4) is rotation-invariant and $\mathcal{IG}_{SO(3)}$ in Equation (5) is a linear combination of *characters* of $SO(3)$, which are *class functions* due to the permutation invariance of trace operations (see Appendix B and C.3). Consider the following diffusion kernel with the equivariant origin selection mechanism in Equation (19):

$$P_{t|0}(g|g_0, O^{(s)}, O^{(b)}) = \int_{\mathbb{R}^3} d\mathbf{p}_{ref} P_{origin}(\mathbf{p}_{ref}|g_0^{-1} \cdot O^{(s)}, O^{(b)}) \mathcal{B}_t((g_0 \triangleleft \mathbf{p}_{ref})^{-1} (g \triangleleft \mathbf{p}_{ref}))$$

where $\triangleleft \mathbf{p}_{ref} : SE(3) \rightarrow SE(3)$ denotes the right action of a pure translation $\mathbf{p}_{ref} \in \mathbb{R}^3$ onto $g = (\mathbf{p}, R) \in SE(3)$ such that

$$g \triangleleft \mathbf{p}_{ref} = \begin{bmatrix} R & \mathbf{p} \\ \emptyset & 1 \end{bmatrix} \begin{bmatrix} I & \mathbf{p}_{ref} \\ \emptyset & 1 \end{bmatrix} = \begin{bmatrix} R & R \mathbf{p}_{ref} + \mathbf{p} \\ \emptyset & 1 \end{bmatrix}$$

Note that the following equation holds for all $g_1, g_2 \in SE(3)$ and $\mathbf{p}_{ref} \in \mathbb{R}^3$:

$$\begin{aligned} (g_1 g_2) \triangleleft \mathbf{p}_{ref} &= \begin{bmatrix} R_1 & \mathbf{p}_1 \\ \emptyset & 1 \end{bmatrix} \begin{bmatrix} R_2 & \mathbf{p}_2 \\ \emptyset & 1 \end{bmatrix} \begin{bmatrix} I & \mathbf{p}_{ref} \\ \emptyset & 1 \end{bmatrix} \\ &= \begin{bmatrix} R_1 R_2 & R_1 (R_2 \mathbf{p}_{ref} + \mathbf{p}_2) + \mathbf{p}_1 \\ \emptyset & 1 \end{bmatrix} \\ &= \begin{bmatrix} R_1 & \mathbf{p}_1 \\ \emptyset & 1 \end{bmatrix} \begin{bmatrix} I & g_2 \mathbf{p}_{ref} \\ \emptyset & 1 \end{bmatrix} \begin{bmatrix} R_2 & \mathbf{0} \\ \emptyset & 1 \end{bmatrix} \\ &= (g_1 \triangleleft (g_2 \mathbf{p}_{ref})) \Delta R_2 \end{aligned} \quad (41)$$

The bi-equivariance of $P_{t|0}$ can be proved using Equation (40) and Equation (41).

Proof. The proof of left equivariance is straightforward as $g_0^{-1} \cdot O^{(s)} = (\Delta g g_0)^{-1} \cdot (\Delta g \cdot O^{(s)})$. The proof of right equivariance is as follows:

$$\begin{aligned} P_{t|0}(g \Delta g^{-1} | g_0 \Delta g^{-1}, O^{(s)}, \Delta g \cdot O^{(b)}) &= \int_{\mathbb{R}^3} d\mathbf{p}_{ref} P_{origin}(\mathbf{p}_{ref}|(\Delta g g_0^{-1}) \cdot O^{(s)}, \Delta g \cdot O^{(b)}) \mathcal{B}_t(((g_0 \Delta g^{-1}) \triangleleft \mathbf{p}_{ref})^{-1} ((g \Delta g^{-1}) \triangleleft \mathbf{p}_{ref})) \\ &= \int_{\mathbb{R}^3} d\mathbf{p}_{ref} P_{origin}(\Delta g^{-1} \mathbf{p}_{ref}|g_0^{-1} \cdot O^{(s)}, O^{(b)}) \mathcal{B}_t(((g_0 \Delta g^{-1}) \triangleleft \mathbf{p}_{ref})^{-1} ((g \Delta g^{-1}) \triangleleft \mathbf{p}_{ref})) \\ &\quad (\because \text{Equation (19)}) \\ &= \int_{\mathbb{R}^3} d\mathbf{p}_{ref} P_{origin}(\Delta g^{-1} \mathbf{p}_{ref}|g_0^{-1} \cdot O^{(s)}, O^{(b)}) \mathcal{B}_t(\Delta R (g_0 \triangleleft (\Delta g^{-1} \mathbf{p}_{ref}))^{-1} (g \triangleleft (\Delta g^{-1} \mathbf{p}_{ref})) \Delta R^{-1}) \\ &\quad (\because \text{Equation (41)}) \\ &= \int_{\mathbb{R}^3} d\mathbf{p}_{ref} P_{origin}(\Delta g^{-1} \mathbf{p}_{ref}|g_0^{-1} \cdot O^{(s)}, O^{(b)}) \mathcal{B}_t((g_0 \triangleleft (\Delta g^{-1} \mathbf{p}_{ref}))^{-1} (g \triangleleft (\Delta g^{-1} \mathbf{p}_{ref}))) \\ &\quad (\because \text{Equation (40)}) \\ &= \int_{\mathbb{R}^3} d\mathbf{p}_{ref} P_{origin}(\mathbf{p}_{ref}|g_0^{-1} \cdot O^{(s)}, O^{(b)}) \mathcal{B}_t((g_0 \triangleleft (\mathbf{p}_{ref}))^{-1} (g \triangleleft (\mathbf{p}_{ref}))) \\ &\quad (\because \text{invariance of Euclidean integral under roto-translation, } \mathbf{p}_{ref} \rightarrow \Delta g \mathbf{p}_{ref}) \\ &= P_{t|0}(g|g_0, O^{(s)}, O^{(b)}) \end{aligned}$$

□

C.6 Derivation of Equation (21)

We first show that $\mathbf{s}_t^*(g|O^{(s)}, O^{(b)}) = \mathbb{E}_{g_0, g_{ref}|g, O^{(s)}, O^{(b)}} [\nabla \log K_t(g_{ref}^{-1} g_0^{-1} g g_{ref})]$ using a simple variational calculus.

Proof. Let $\delta \mathbf{s}_t(g|O^{(s)}, O^{(b)})$ be a perturbation of the score model $\mathbf{s}_t(g|O^{(s)}, O^{(b)})$. For the optimal score model $\mathbf{s}_t^*(g|O^{(s)}, O^{(b)})$, any small perturbation would result in zero perturbation of the objective.

$$\begin{aligned} \mathbf{s}_t^*(g|O^{(s)}, O^{(b)}) &= \arg \min_{\mathbf{s}_t(g|O^{(s)}, O^{(b)})} \mathcal{J}_t [\mathbf{s}_t(g|O^{(s)}, O^{(b)})] \\ \Rightarrow \delta \mathcal{J}_t [\mathbf{s}_t^*(g|O^{(s)}, O^{(b)})] &= 0 \quad \forall \delta \mathbf{s}_t^*(g|O^{(s)}, O^{(b)}) \end{aligned}$$

The explicit form of the perturbation of the objective with regard to $\delta \mathbf{s}_t(g|O^{(s)}, O^{(b)})$ is written as follows:

$$\begin{aligned} \delta \mathcal{J}_t [\mathbf{s}_t(g|O^{(s)}, O^{(b)})] &= \delta \left(\mathbb{E}_{g, g_0, g_{ref}, O^{(s)}, O^{(b)}} \left[\frac{1}{2} \left\| \mathbf{s}_t(g|O^{(s)}, O^{(b)}) - \nabla \log K_t(g_{ref}^{-1} g_0^{-1} g g_{ref}) \right\|^2 \right] \right) \\ &= \mathbb{E}_{g, O^{(s)}, O^{(b)}} \left[\delta \mathbf{s}_t(g|O^{(s)}, O^{(b)}) \cdot \left[\mathbf{s}_t(g|O^{(s)}, O^{(b)}) - \mathbb{E}_{g_0, g_{ref}|g, O^{(s)}, O^{(b)}} [\nabla \log K_t(g_{ref}^{-1} g_0^{-1} g g_{ref})] \right] \right] \end{aligned}$$

Therefore, assuming $P_t(g|O^{(s)}, O^{(b)}) > 0 \quad \forall g, O^{(s)}, O^{(b)}$, the optimal score model must be

$$\mathbf{s}_t^*(g|O^{(s)}, O^{(b)}) = \mathbb{E}_{g_0, g_{ref}|g, O^{(s)}, O^{(b)}} [\nabla \log K_t(g_{ref}^{-1} g_0^{-1} g g_{ref})]$$

□

We now show that $\mathbb{E}_{g_0, g_{ref}|g, O^{(s)}, O^{(b)}} [\nabla \log K_t(g_{ref}^{-1} g_0^{-1} g g_{ref})] = \nabla \log P_t(g|O^{(s)}, O^{(b)})$.

Proof.

$$\begin{aligned} &\mathbb{E}_{g_0, g_{ref}|g, O^{(s)}, O^{(b)}} [\nabla \log K_t(g_{ref}^{-1} g_0^{-1} g g_{ref})] \\ &= \int dg_0 \int dg_{ref} P(g_0, g_{ref}|g, O^{(s)}, O^{(b)}; t) \frac{\nabla K_t(g_{ref}^{-1} g_0^{-1} g g_{ref})}{K_t(g_{ref}^{-1} g_0^{-1} g g_{ref})} \\ &= \int dg_0 \int dg_{ref} \left[P(g|g_0, g_{ref}, O^{(s)}, O^{(b)}; t) \frac{P(g_0, g_{ref}|O^{(s)}, O^{(b)})}{P_t(g|O^{(s)}, O^{(b)})} \right] \frac{\nabla K_t(g_{ref}^{-1} g_0^{-1} g g_{ref})}{K_t(g_{ref}^{-1} g_0^{-1} g g_{ref})} \\ &= \int dg_0 \int dg_{ref} \underbrace{P(g|g_0, g_{ref}, O^{(s)}, O^{(b)}; t)}_{\nabla P_t(g|O^{(s)}, O^{(b)})} \frac{P(g_0, g_{ref}|O^{(s)}, O^{(b)})}{P_t(g|O^{(s)}, O^{(b)})} \frac{\nabla K_t(g_{ref}^{-1} g_0^{-1} g g_{ref})}{\underbrace{K_t(g_{ref}^{-1} g_0^{-1} g g_{ref})}_{\nabla K_t(g|O^{(s)}, O^{(b)})}} \\ &\quad (\because P(g|g_0, g_{ref}, O^{(s)}, O^{(b)}; t) = P(g|g_0, g_{ref}; t) = K_t(g_{ref}^{-1} g_0^{-1} g g_{ref})) \\ &= \frac{1}{P_t(g|O^{(s)}, O^{(b)})} \int dg_0 \int dg_{ref} P(g_0, g_{ref}|O^{(s)}, O^{(b)}) \nabla K_t(g_{ref}^{-1} g_0^{-1} g g_{ref}) \\ &= \frac{1}{P_t(g|O^{(s)}, O^{(b)})} \nabla \int dg_0 \int dg_{ref} P(g_0, g_{ref}|O^{(s)}, O^{(b)}) K_t(g_{ref}^{-1} g_0^{-1} g g_{ref}) \\ &= \frac{1}{P_t(g|O^{(s)}, O^{(b)})} \nabla \int dg_0 P_0(g_0|O^{(s)}, O^{(b)}) \int dg_{ref} P(g_{ref}|g_0^{-1} \cdot O^{(s)}, O^{(b)}) K_t(g_{ref}^{-1} g_0^{-1} g g_{ref}) \\ &= \frac{1}{P_t(g|O^{(s)}, O^{(b)})} \nabla P_t(g|O^{(s)}, O^{(b)}) \quad (\because \text{Equation (16) and Equation (13)}) \\ &= \frac{\nabla P_t(g|O^{(s)}, O^{(b)})}{P_t(g|O^{(s)}, O^{(b)})} = \nabla \log P_t(g|O^{(s)}, O^{(b)}) \end{aligned}$$

□

Therefore, we prove that $\mathbf{s}_t^*(g|O^{(s)}, O^{(b)}) = \nabla \log P_t(g|O^{(s)}, O^{(b)})$.

C.7 Proof of Proposition 5

For readers' convenience, we reproduce the bi-equivariance conditions for the score functions in Proposition 1 with explicit components.

$$\mathbf{s}(\Delta g g | \Delta g \cdot O^{(s)}, O^{(b)}) = \mathbf{s}(g | O^{(s)}, O^{(b)}) \quad (42)$$

$$\begin{aligned} \mathbf{s}(g \Delta g^{-1} | O^{(s)}, \Delta g \cdot O^{(b)}) &= [\text{Ad}_{\Delta g}]^{-T} \mathbf{s}(g | O^{(s)}, O^{(b)}) \\ &= \begin{bmatrix} \Delta R & \emptyset \\ [\Delta \mathbf{p}]^\wedge \Delta R & \Delta R \end{bmatrix} \begin{bmatrix} \mathbf{s}_\nu(g | O^{(s)}, O^{(b)}) \\ \mathbf{s}_\omega(g | O^{(s)}, O^{(b)}) \end{bmatrix} \\ &= \Delta R \mathbf{s}_\nu(g | O^{(s)}, O^{(b)}) \oplus \left[\Delta R \mathbf{s}_\omega(g | O^{(s)}, O^{(b)}) + \Delta \mathbf{p} \times \Delta R \mathbf{s}_\nu(g | O^{(s)}, O^{(b)}) \right] \end{aligned} \quad (43)$$

where we used the fact that the inverse transpose of the adjoint matrix is as follows [35, 37]:

$$[\text{Ad}_{\Delta g}]^{-T} = \begin{bmatrix} \Delta R & \emptyset \\ [\Delta \mathbf{p}]^\wedge \Delta R & \Delta R \end{bmatrix}$$

We begin by proving the bi-equivariance of the linear (translational) score term

Proof. The left invariance of the linear score model is proved as

$$\begin{aligned} \mathbf{s}_{\nu;t}(\Delta g g | \Delta g \cdot O^{(s)}, O^{(b)}) &= \int_{\mathbb{R}^3} d^3 \mathbf{x} \rho_{\nu;t}(\mathbf{x} | O^{(b)}) \tilde{\mathbf{s}}_{\nu;t}(\Delta g g, \mathbf{x} | \Delta g \cdot O^{(s)}, O^{(b)}) \\ &= \int_{\mathbb{R}^3} d^3 \mathbf{x} \rho_{\nu;t}(\mathbf{x} | O^{(b)}) \tilde{\mathbf{s}}_{\nu;t}(g, \mathbf{x} | O^{(s)}, O^{(b)}) \quad (\because \text{Equation (26)}) \\ &= \mathbf{s}_{\nu;t}(g | O^{(s)}, O^{(b)}) \end{aligned}$$

The right equivariance of the linear score model is proved as

$$\begin{aligned} \mathbf{s}_{\nu;t}(g \Delta g^{-1} | O^{(s)}, \Delta g \cdot O^{(b)}) &= \int_{\mathbb{R}^3} d^3 \mathbf{x} \rho_{\nu;t}(\mathbf{x} | \Delta g \cdot O^{(b)}) \tilde{\mathbf{s}}_{\nu;t}(g \Delta g^{-1}, \mathbf{x} | O^{(s)}, \Delta g \cdot O^{(b)}) \\ &= \int_{\mathbb{R}^3} d^3 \mathbf{x} \rho_{\nu;t}(\Delta g \mathbf{x} | \Delta g \cdot O^{(b)}) \tilde{\mathbf{s}}_{\nu;t}(g \Delta g^{-1}, \Delta g \mathbf{x} | O^{(s)}, \Delta g \cdot O^{(b)}) \\ &\quad (\because \text{invariance of Euclidean integral under roto-translation } \mathbf{x} \rightarrow \Delta g \mathbf{x}) \\ &= \int_{\mathbb{R}^3} d^3 \mathbf{x} \rho_{\nu;t}(\mathbf{x} | O^{(b)}) \Delta R \tilde{\mathbf{s}}_{\nu;t}(g, \mathbf{x} | O^{(s)}, O^{(b)}) \quad (\because \text{Equation (25) and Equation (27)}) \\ &= \Delta R \int_{\mathbb{R}^3} d^3 \mathbf{x} \rho_{\nu;t}(\mathbf{x} | O^{(b)}) \tilde{\mathbf{s}}_{\nu;t}(g, \mathbf{x} | O^{(s)}, O^{(b)}) \\ &= \Delta R \mathbf{s}_{\nu;t}(g | O^{(s)}, O^{(b)}) \end{aligned}$$

□

Let the angular (rotational) score model be decomposed into the spin term $\mathbf{s}_{\text{spin};t}$ and the orbital term $\mathbf{s}_{\text{orbital};t}$ as in Equation (24). The bi-equivariance of spin term in the angular (rotational) score model

$$\begin{aligned} \mathbf{s}_{\text{spin};t}(g | O^{(s)}, O^{(b)}) &= \int_{\mathbb{R}^3} d^3 \mathbf{x} \rho_{\omega;t}(\mathbf{x} | O^{(b)}) \tilde{\mathbf{s}}_{\omega;t}(g, \mathbf{x} | O^{(s)}, O^{(b)}) \\ \mathbf{s}_{\text{spin};t}(\Delta g g | \Delta g \cdot O^{(s)}, O^{(b)}) &= \mathbf{s}_{\text{spin};t}(g | O^{(s)}, O^{(b)}) \\ \mathbf{s}_{\text{spin};t}(g \Delta g^{-1} | O^{(s)}, \Delta g \cdot O^{(b)}) &= \Delta R \mathbf{s}_{\text{spin};t}(g | O^{(s)}, O^{(b)}) \end{aligned}$$

can be proven in a similar fashion to the linear score model. It can be shown that the orbital term satisfies the following bi-equivariance condition

$$\begin{aligned} \mathbf{s}_{\text{orbital};t}(g | O^{(s)}, O^{(b)}) &= \int_{\mathbb{R}^3} d^3 \mathbf{x} \rho_{\nu;t}(\mathbf{x} | O^{(b)}) \mathbf{x} \times \tilde{\mathbf{s}}_{\nu;t}(g, \mathbf{x} | O^{(s)}, O^{(b)}) \\ \mathbf{s}_{\text{orbital};t}(\Delta g g | \Delta g \cdot O^{(s)}, O^{(b)}) &= \mathbf{s}_{\text{orbital};t}(g | O^{(s)}, O^{(b)}) \\ \mathbf{s}_{\text{orbital};t}(g \Delta g^{-1} | O^{(s)}, \Delta g \cdot O^{(b)}) &= \Delta \mathbf{p} \times \Delta R \mathbf{s}_{\text{orbital};t}(g | O^{(s)}, O^{(b)}) \end{aligned}$$

Proof. The left invariance is straightforward, as the linear score field $\tilde{s}_{\nu;t}$ is left-invariant as Equation (26). The right equivariance can be proved as follows

$$\begin{aligned}
& \mathbf{s}_{\text{orbital};t}(g \Delta g^{-1} | O^{(s)}, \Delta g \cdot O^{(b)}) \\
&= \int_{\mathbb{R}^3} d^3 \mathbf{x} \rho_{\nu;t}(\mathbf{x} | \Delta g \cdot O^{(b)}) \mathbf{x} \times \tilde{s}_{\nu;t}(g \Delta g^{-1}, \mathbf{x} | O^{(s)}, \Delta g \cdot O^{(b)}) \\
&= \int_{\mathbb{R}^3} d^3 \mathbf{x} \rho_{\nu;t}(\Delta g^{-1} \mathbf{x} | O^{(b)}) \mathbf{x} \times \Delta R \tilde{s}_{\nu;t}(g, \Delta g^{-1} \mathbf{x} | O^{(s)}, O^{(b)}) \\
&\quad (\because \text{Equation (25) and Equation (27)}) \\
&= \int_{\mathbb{R}^3} d^3 \mathbf{x} \rho_{\nu;t}(\mathbf{x} | O^{(b)}) (\Delta R \mathbf{x} + \Delta \mathbf{p}) \times \Delta R \tilde{s}_{\nu;t}(g, \mathbf{x} | O^{(s)}, O^{(b)}) \\
&\quad (\because \text{invariance of Euclidean integral under roto-translation } \mathbf{x} \rightarrow \Delta g \mathbf{x} = \Delta R \mathbf{x} + \Delta \mathbf{p}) \\
&= \Delta R \left[\int_{\mathbb{R}^3} d^3 \mathbf{x} \rho_{\nu;t}(\mathbf{x} | O^{(b)}) \mathbf{x} \times \tilde{s}_{\nu;t}(g, \mathbf{x} | O^{(s)}, O^{(b)}) \right] \\
&\quad + \Delta \mathbf{p} \times \Delta R \int_{\mathbb{R}^3} d^3 \mathbf{x} \rho_{\nu;t}(\mathbf{x} | O^{(b)}) \tilde{s}_{\nu;t}(g, \mathbf{x} | O^{(s)}, O^{(b)}) \\
&\quad (\because R \mathbf{x} \times R \mathbf{y} = R(\mathbf{x} \times \mathbf{y}) \quad \forall \mathbf{x}, \mathbf{y} \in \mathbb{R}^3) \\
&= \Delta R \mathbf{s}_{\text{orbital};t}(g | O^{(s)}, O^{(b)}) + \Delta \mathbf{p} \times \Delta R \mathbf{s}_{\nu;t}(g | O^{(s)}, O^{(b)})
\end{aligned}$$

□

As a result, the angular (rotational) score model

$$\mathbf{s}_{\omega;t}(g | O^{(s)}, O^{(b)}) = \mathbf{s}_{\text{orbital};t}(g | O^{(s)}, O^{(b)}) + \mathbf{s}_{\text{spin};t}(g | O^{(s)}, O^{(b)})$$

satisfies the following bi-equivariance

$$\begin{aligned}
\mathbf{s}_{\omega;t}(\Delta g | \Delta g \cdot O^{(s)}, O^{(b)}) &= \mathbf{s}_{\omega;t}(g | O^{(s)}, O^{(b)}) \\
\mathbf{s}_{\omega;t}(g \Delta g^{-1} | O^{(s)}, \Delta g \cdot O^{(b)}) &= \Delta R \left[\mathbf{s}_{\text{orbital};t}(g | O^{(s)}, O^{(b)}) + \mathbf{s}_{\text{spin};t}(g | O^{(s)}, O^{(b)}) \right] \\
&\quad + \Delta \mathbf{p} \times \Delta R \mathbf{s}_{\nu;t}(g | O^{(s)}, O^{(b)}) \\
&= \Delta R \mathbf{s}_{\omega;t}(g | O^{(s)}, O^{(b)}) + \Delta \mathbf{p} \times \Delta R \mathbf{s}_{\nu;t}(g | O^{(s)}, O^{(b)})
\end{aligned}$$

Hence, we have proven Proposition 5 that the score model in Equation (22) is bi-equivariant, satisfying Equation (42) and Equation (43).

C.8 Proof of Proposition 6

Proof.

$$\begin{aligned}
& \tilde{s}_{\square;t}(\Delta g g, \mathbf{x} | \Delta g \cdot O^{(s)}, O^{(b)}) \\
&= \psi_{\square;t}(\mathbf{x} | O^{(b)}) \otimes_{\square;t}^{(\rightarrow 1)} \mathbf{D}(R^{-1} \Delta R^{-1}) \varphi_{\square;t}(\Delta g g \mathbf{x} | \Delta g \cdot O^{(s)}) \\
&= \psi_{\square;t}(\mathbf{x} | O^{(b)}) \otimes_{\square;t}^{(\rightarrow 1)} \mathbf{D}(R^{-1} \Delta R^{-1}) \mathbf{D}(\Delta R) \varphi_{\square;t}(g \mathbf{x} | O^{(s)}) \quad (\because \text{Equation (2)}) \\
&= \psi_{\square;t}(\mathbf{x} | O^{(b)}) \otimes_{\square;t}^{(\rightarrow 1)} \mathbf{D}(R^{-1} \Delta R^{-1} \Delta R) \varphi_{\square;t}(g \mathbf{x} | O^{(s)}) \quad (\because \text{Equation (1)}) \\
&= \tilde{s}_{\square;t}(g, \mathbf{x} | O^{(s)}, O^{(b)})
\end{aligned}$$

$$\begin{aligned}
& \tilde{s}_{\square;t}(g \Delta g^{-1}, \Delta g \mathbf{x} | O^{(s)}, \Delta g \cdot O^{(b)}) \\
&= \psi_{\square;t}(\Delta g \mathbf{x} | \Delta g \cdot O^{(b)}) \otimes_{\square;t}^{(\rightarrow 1)} \mathbf{D}(\Delta R R^{-1}) \varphi_{\square;t}(g \cancel{\Delta g^{-1} \Delta g} \mathbf{x} | O^{(s)}) \\
&= \mathbf{D}(\Delta R) \psi_{\square;t}(\mathbf{x} | O^{(b)}) \otimes_{\square;t}^{(\rightarrow 1)} \mathbf{D}(\Delta R R^{-1}) \varphi_{\square;t}(g \mathbf{x} | O^{(s)}) \quad (\because \text{Equation (2)}) \\
&= \mathbf{D}(\Delta R) \psi_{\square;t}(\mathbf{x} | O^{(b)}) \otimes_{\square;t}^{(\rightarrow 1)} \mathbf{D}(\Delta R) \mathbf{D}(R^{-1}) \varphi_{\square;t}(g \mathbf{x} | O^{(s)}) \quad (\because \text{Equation (1)}) \\
&= \mathbf{D}^{(1)}(\Delta R) \left[\psi_{\square;t}(\mathbf{x} | O^{(b)}) \otimes_{\square;t}^{(\rightarrow 1)} \mathbf{D}(R^{-1}) \varphi_{\square;t}(g \mathbf{x} | O^{(s)}) \right] \\
&\quad (\because [\mathbf{D}(R)\mathbf{v}] \otimes^{(\rightarrow l)} [\mathbf{D}(R)\mathbf{w}] = \mathbf{D}^{(l)}(R) [\mathbf{v} \otimes^{(\rightarrow l)} \mathbf{w}]) \\
&= \Delta R \tilde{s}_{\square;t}(g, \mathbf{x} | O^{(s)}, O^{(b)})
\end{aligned}$$

where in the last line we assume that the degree-1 Wigner D-matrix $\mathbf{D}^{(1)}(\cdot)$ is in the real basis with $x - y - z$ axis ordering. Note that the last line only holds in this specific choice of basis. Therefore, the type-1 or higher descriptors of the two EDFs must be defined in this basis. \square